Molecular Therapy
Methods & Clinical Development
Original Article

CRISPR-Cas9 correction in the DMD mouse model is accompanied by upregulation of Dp71f protein

Tatiana V. Egorova,[1,2] Anna V. Polikarpova,[1,2] Svetlana G. Vassilieva,[1] Marina A. Dzhenkova,[1] Irina M. Savchenko,[3] Oleg A. Velyaev,[1] Anna A. Shmidt,[1,3] Vladislav O. Soldatov,[4] Mikhail V. Pokrovskii,[4] Alexey V. Deykin,[2,5] and Maryana V. Bardina[1,2,3]

[1]Laboratory of Modeling and Therapy of Hereditary Diseases, Institute of Gene Biology, Russian Academy of Sciences, Moscow 119334, Russia; [2]Marlin Biotech LLC, Sochi 354340, Russia; [3]Center for Precision Genome Editing and Genetic Technologies for Biomedicine, Institute of Gene Biology Russian Academy of Sciences, Moscow 119334, Russia; [4]Research Institute of Living Systems Pharmacology, Belgorod National Research University, Belgorod 308007, Russia; [5]Joint Center for Genetic Technologies, Laboratory of Genetic Technologies and Gene Editing for Biomedicine and Veterinary Medicine, Department of Pharmacology and Clinical Pharmacology, Belgorod National Research University, Belgorod 308015, Russia

Duchenne muscular dystrophy (DMD) is a severe hereditary disease caused by a deficiency in the dystrophin protein. The most frequent types of disease-causing mutations in the DMD gene are frameshift deletions of one or more exons. Precision genome editing systems such as CRISPR-Cas9 have shown potential to restore open reading frames in numerous animal studies. Here, we applied an AAV-CRISPR double-cut strategy to correct a mutation in the DMD mouse model with exon 8–34 deletion, encompassing the N-terminal actin-binding domain. We report successful excision of the 100-kb genomic sequence, which includes exons 6 and 7, and partial improvement in cardiorespiratory function. While corrected mRNA was abundant in muscle tissues, only a low level of truncated dystrophin was produced, possibly because of protein instability. Furthermore, CRISPR-Cas9-mediated genome editing upregulated the Dp71f dystrophin isoform on the sarcolemma. Given the previously reported Dp71-associated muscle pathology, our results question the applicability of genome editing strategies for some DMD patients with N-terminal mutations. The safety and efficacy of CRISPR-Cas9 constructs require rigorous investigation in patient-specific animal models.

INTRODUCTION

Two muscular diseases, Duchenne muscular dystrophy (DMD) and Becker muscular dystrophy (BMD), are caused by mutations in the *DMD* gene located on the X chromosome. The *DMD* gene (~2.4 Mb) is the largest known human gene, comprised of 79 exons. Seven independent promoters result in three full-length isoforms and at least four N-terminally truncated proteins. Alternative splicing and polyadenylation signals further increase the possible number of isoforms.[1] The major splice variant is expressed in muscles and encodes 427-kDa dystrophin (isoform Dp427m). Muscular dystrophin plays a vital role in maintaining the integrity of myofibers. Dp427m consists of four superdomains: the N-terminal actin-binding domain (N-ABD; encoded by exons 1–8), the central rod domain (exons 8–64), the cysteine-rich (CR) domain (exons 64–70), and the C-terminal (CT) domain (exons 71–79).[2] The rod domain is composed of 24 spectrin-like repeats (SR1–SR24) interspersed by four hinges (H1–H4). The N-terminal portion of the protein (N-ABD and SR11–-15) binds to the intracellular actin filaments, the CT region associates with the cytoplasmic face of the sarcolemma, and the rod domain acts as a flexible linker. The CR and CT domains nucleate the assembly of the transmembrane dystrophin-associated glycoprotein complex (DAGC) on the sarcolemma.[2] Besides dystrophin, the DAGC includes multiple structural and signaling proteins: sarcoglycans, dystroglycans, sarcospan, syntrophins, dystrobrevin, and neuronal nitric oxide synthase. Dystrophin and the DAGC bridge the muscle cytoskeleton to the extracellular matrix. These interactions stabilize the sarcolemma and protect muscle fibers from damage induced by repeated contractions. Dystrophin-disrupting mutations result in loss of the DAGC on the sarcolemma and lead to muscular dystrophy, characterized by progressive muscle wasting and replacement by fat and fibrosis.[2]

Deletions spanning one or multiple exons are the most common *DMD* mutations responsible for muscular dystrophies and account for 60%–70% of DMD cases and 80%–85% of BMD cases.[3] Two hotspots of the disease-causing mutations were identified in exons 2–20 and exons 45–55.[4] DMD is caused by mutations that disrupt the reading frame and give rise to premature stop codons. Transcripts with such mutations are prone to nonsense-mediated decay, and the truncated proteins lacking the CT portion of dystrophin are non-functional and subject to degradation. The absence of the full-length Dp427m affects young boys, who experience severe manifestations, including cardiac and respiratory dysfunction, leading to death in the thirties. In contrast, BMD is caused by in-frame deletions accompanied by synthesis of an internally truncated but partially

Received 10 August 2022; accepted 14 June 2023;
https://doi.org/10.1016/j.omtm.2023.06.006.

Correspondence: Tatiana V. Egorova, Laboratory of Modeling and Therapy of Hereditary Diseases, Institute of Gene Biology, Russian Academy of Sciences, Vavilova 34/5, 119334 Moscow, Russia.
E-mail: egorovatv@genebiology.ru

functional dystrophin. Therefore, BMD has later onset and milder manifestations with preserved ambulation until old age.[2]

Some of the first nucleic acid-based drugs to target DMD are oligonucleotides that induce exon skipping.[5] Antisense oligonucleotides bind in a sequence-specific manner to the *DMD* pre-mRNA and induce exon exclusion, compensating for out-of-frame deletion. No changes are introduced in the patient's *DMD* genomic sequence; therefore, the therapeutic effect is transient, and repeated treatment is required.[6] Skipping of a single exon by phosphorodiamidate morpholino oligonucleotide (PMO) has demonstrated efficiency in animal models[7,8] and reached clinical application.[9] Alternatively, gene therapy can be applied to deliver an exogenous copy of a functional gene or to correct the endogenous *DMD* for long-term effects.[10–12] Gene replacement therapy aims to deliver, via viral vectors, a shortened dystrophin coding sequence (microdystrophin) to affected tissues. Several drug candidates with various microdystrophin configurations have been tested in clinical trials and demonstrate promising results.[13] Mutation-specific genome editing restores the reading frame of the endogenous dystrophin. CRISPR-Cas9-based technologies induce targeted cuts into the *DMD* genomic sequence.[11] Single cutting achieves exon reframing by introducing insertions or deletions (indels) with an appropriate number of nucleotides.[14,15] Similar to oligonucleotides, single-cut gene editing has also been applied for splicing modulation and inducing skipping of the targeted exon.[14,15] Two cooperative cuts allow removal of one or more exons (exon excision).[16,17] Additional enzyme or sequence delivery with a genome editing complex has been tested to introduce precise corrections in the *Dmd* gene.[18,19]

Antisense, gene replacement, and genome editing therapies are similar in supplying the patient's muscles with the functional shortened dystrophin and expectedly converting severe DMD to milder BMD. The gene replacement strategy is universal for all mutation types, which is an advantage over mutation-specific antisense oligos and genome editing. However, exogenous microdystrophin does not integrate into the genome, and the genetic material persists in the nucleus in the form of an episome, meaning that the duration of the therapeutic effect is in inverse correlation with the cell division rate.[20] When applied, genome editing leads to permanent modification of the *DMD* gene with formation of BMD-like mutations. Unlike gene replacement methods that rely on the regulatory elements in the vector, genome editing allows expression of the corrected dystrophin gene with natural tissue specificity, timing, and levels. Expression of dystrophin from an endogenous locus is also preserved when exon skipping is induced by antisense oligonucleotides.[21] However, to maintain the therapeutic effect, continuous drug application is needed. Moreover, limited drug biodistribution to muscular organs, such as the heart and diaphragm, necessitates development of novel oligonucleotide modifications. Experiments on model animals have demonstrated the applicability of oligonucleotides for multiple-exon skipping,[6] but their efficacy is expectedly lower than that for single-exon skipping. The genome editing approach bears the potential for multiple exon exclusion, which has been demonstrated in several *in vivo* studies on DMD animal models.[12,22]

In the current work, we explored the potential of CRISPR-Cas9-mediated genome editing to repair an out-of-frame deletion of exons 8–34 of the *DMD* gene reported in a Russian DMD patient.[23] The mutation spans a portion of the gene encoding for the N-ABD domain and nearly half of the rod domain (SR1–SR11) and causes formation of a premature stop codon in exon 35. We induced CRISPR-Cas9-mediated double-cutting to excise exons 6 and 7 and to restore the dystrophin reading frame. The mouse model DMDdel8–34, recapitulating patient-specific mutation, enables testing the efficacy of the technology.[23] The primary concern is the functionality of the corrected dystrophin missing F-actin-binding elements from the N-ABD and the rod domains. Another challenge is the efficiency of the CRISPR-Cas9-mediated double-cut technology, which is predictably less effective than single cutting. Underscoring the complexity of the approach, no studies have yet reported CRISPR-Cas9-mediated exon excision to correct N-terminal multi-exon deletions affecting the N-ABD domain *in vivo*.

RESULTS

Double-cut genome editing restored the reading frame *in vitro* in muscle cells with *Dmd* deleted exons 8–34

DMDdel8–34 mice lack dystrophin protein because of exon 8–34 deletion and a consequent reading frame shift with premature stop codon appearance in exon 35. For reading frame restoration, we applied a double-cut strategy, employing AAVs to deliver *Staphylococcus aureus* Cas9 (SaCas9) and guide RNAs (gRNAs) to exon 6 and 7 flanking sequences located in the fifth intron and chimeric introns 7–34, respectively. Application of these editing complexes aimed to excise an additional 100 kb from the murine *Dmd* gene. To minimize potential off-target effects, we designed gRNAs with limited predicted off-target sites in the murine genome. Three guides for each intron were selected (Figure 1A), designated here as 5in1–3 and 34in1–3 (Table S1). Corresponding guides were subcloned into SaCas9-expressing AAV constructs. First, we tested them *in vitro* pairwise (Figure 1B). AAV-DJ viruses reported previously to be effective *in vitro*[24] were used for transduction of primary myoblast cultures derived from neonatal DMDdel8–34 skeletal muscle. Then, the cells were cultured under differentiation conditions to upregulate dystrophin expression. We detected a corrected *Dmd* transcript bearing a deletion of exons 6–34 (Figure 1C; 530 bp) along with a native mutant form of the transcript with deleted exons 8–34 (Figure 1C; 822 bp). Sanger sequencing of the corresponding cDNA amplicon verified correct splicing of exons 5–35 (Figure 1D). The most effective guides were 5in2, 5in3, 34in2, and 34in3 in all combinations, reaching 30%–50% corrected mRNA expression (Figure 1E).

Genome editing *in vivo* with intramuscular AAV9-CRISPR delivery demonstrated functional improvement

The next round of guide screening for exon 6–7 deletion was performed *in vivo* using intramuscular AAV injections. For robust guide delivery, we selected AAV serotype 9, which effectively targets muscle tissues, including skeletal muscles, diaphragm, and heart, following local or systemic infusions.[25] Four combinations of AAV9 vector pairs encoding Cas9 and guides 5in2, 5in3, 34in2, or 34in3 were

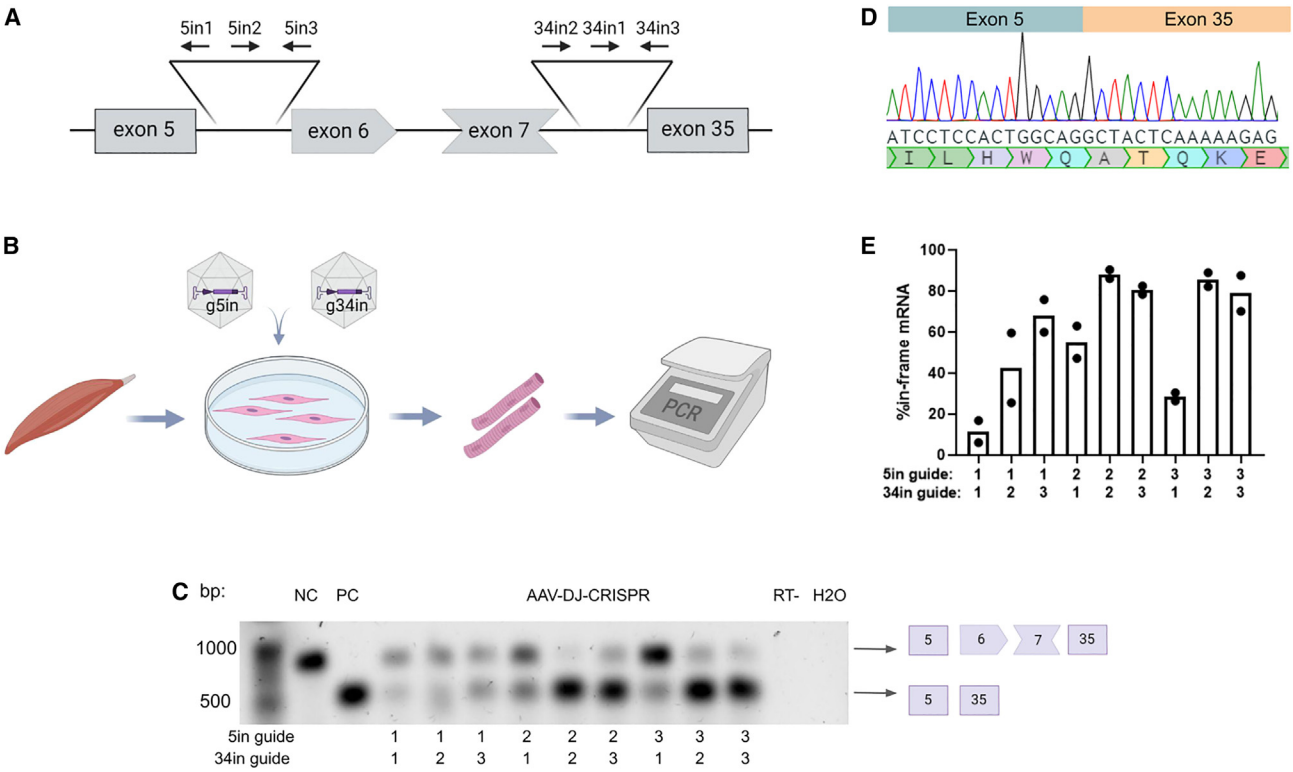

Figure 1. Guide selection to excise exons 6 and 7 in the *Dmd* gene of DMDdel8–34 mice *in vitro*

(A) Illustration showing relative positions of guides designed to target introns 5 and 7/34. (B) Experimental outline for testing guide efficiency *in vitro*. Primary myoblasts derived from skeletal muscle of DMDdel8–34 mice were cotransduced with AAV-DJ encoding genome editing complexes (5E+11 VG of each). Expression analysis was performed by RT-PCR on day 8 after inducing differentiation. (C) Representative image of RT-PCR analysis *in vitro*. Arrows indicate PCR fragments corresponding to *Dmd* transcripts bearing exon 8–34 deletion (800 bp) and corrected transcripts with excised exons 6 and 7 (500 bp). NC, negative control of cells transduced with a nontargeting vector; PC, amplicon from plasmid DNA containing *Dmd* cDNA with deletion of exons 6–34; RT-, control amplification of a sample without revertase. (D) Sanger sequencing confirms restoration of the reading frame in transcripts with deletion of exons 6–34. (E) Quantitative analysis of guide pair efficiency. The percentage of corrected mRNA is shown.

injected into 8-week-old DMDdel8–34 mice at a high dose of 1E+12 vector genomes (VGs) of each per tibialis anterior (TA) muscle (Figure 2). Two weeks post injection, the desired deletion of the 100-kb genomic fragment was detected by PCR amplification in all analyzed tissue samples (Figure S1A). As verified by Sanger sequencing, deletion borders in all four guide combinations perfectly matched predicted blunt-end Cas9 cut sites (Figure 2A). The deconvolution algorithm[26] allowed us to identify alternative sequences containing indels from −29 to +36 bp (Figure S1B). Successful guide combinations led to an expression of up to 63% of the corrected dystrophin transcript (Figure 2B). We detected a convincing level of the target transcripts in all treated samples (Figure S2A) that enriched the total dystrophin mRNA pool (Figure S2B). Immunostaining of muscle cryosections with antibodies specific to the dystrophin C terminus confirmed localization of the protein on the sarcolemma (Figure 2C). Dystrophin-positive fibers ranged between 48% and 74% for different guide combinations (Figure S2C).

As a proof of concept for the selected editing strategy, we compared the force of the TA muscle in CRISPR-Cas9-treated groups with the wild-type control. Different combinations of guides to varying degrees led to TA muscle recovery, as assessed by the repeated lengthening contractions and specific force test (Figures S2D and S2E). Notably, specific muscle strength correlated well with the percentage of dystrophin-positive fibers (Figure S2F). Based on these results, we selected the two most promising guide combinations (5in3+34in2 and 5in3+34in3). To refine the screening data, we repeated the TA injection and functional recovery experiments. Following seven repeated contractions, the force deficit in the saline-treated DMDdel8–34 mice reached 83.6% compared with 59.4% in the healthy control group (Figure 2D). A significant reduction of the force deficit (53.2%) was observed in animals treated with 5in3+34in2 (Figure 2D), in line with previous results (Figure S2D). The specific force test did not demonstrate significant changes in either of the CRISPR-Cas9-treated groups (Figure 2E); however, the recovery was seemingly better with 5in3+34in2 (Figures 2E and S2E). Comparing genome editing efficiency and functional outcome, we showed that improvements in TA strength correlate with the copy number of the edited transcript detected in the muscle (Figure 2F).

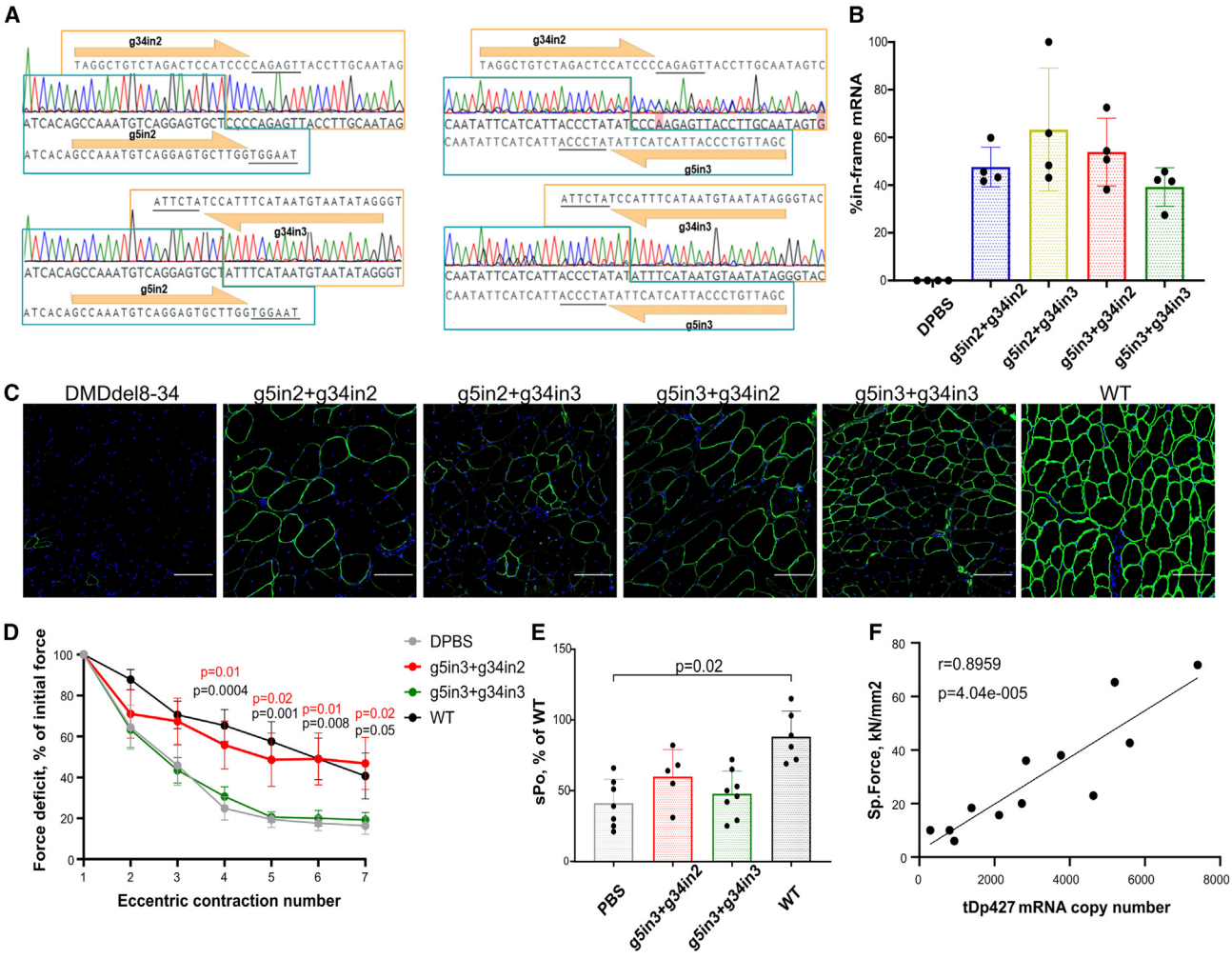

Figure 2. Comparison of genome editing efficiency and functional outcome for combinations of guides following intramuscular injections

A mix of AAV9 encoding genome editing complexes (1E+12 VG of each) was injected into the tibialis anterior (TA) muscle of 8-week-old DMDdel8–34 mice. Analysis was performed on day 14. (A) Deletion borders in introns 5 and 34 identified by Sanger sequencing. Guides are labeled by arrows, and PAM sites are underlined. See also Figure S1. (B) Percent of edited mRNA revealed by RT-PCR analysis. See also Figures S2A and S2B. Data are presented as the mean ± SD. (C) Immunofluorescence analysis of transverse TA cryosections. Dystrophin is green (Ab15277), and nuclei are counterstained blue. Scale bar, 50 μm. See also Figure S2C. (D) Force deficit of the TA muscle after repeated eccentric contractions. Data are presented as the mean ± SEM; n = 5–8 per group. p values describing differences from the PBS group are indicated. (E) Specific force of TA muscle. Data are presented as the mean ± SD. (F) Correlation analysis of tDp427 transcript copy number vs. specific TA muscle force. Pearson's correlation coefficient (r) and p values are shown.

Results with intramuscular injections proved the feasibility of the *in vivo* double-cut approach for eliminating exons 6 and 7 in mutant dystrophin. Comparison of genome editing efficiency and the muscle recovery of different gRNAs allowed us to define 5in3 + 34in2 as a promising guide combination for gene therapy development.

On-target and off-target activity of selected guides

To evaluate the safety of the proposed CRISPR-Cas9-based approach, we analyzed the off-target activity of guides 5in3 and 34in2 on primary DMDdel8–34 myoblast cell culture. *In vitro* studies allow application of a high virus "dose" and enable detection of rare editing events by conventional lab techniques. First, we estimated the on-target efficiency of guides in the myoblast culture using the T7EI assay. Transduction of myoblasts with a pair of guides resulted in the desired deletion as well as indels at both Cas9 cut sites (Figures S3A–S3C). The single-sgRNA treatment induced indel formation in the target site but not in the recognition site of another guide (Figures S3B and S3C). To quantify on-target editing events, we used TIDE (tracking of indels by decomposition).[27] The average sgRNA efficiency was 31% for 5in3 and 13% for 34in2, respectively, and did not differ between samples transduced by individual guides or with both simultaneously (Figures 3A and 3B).

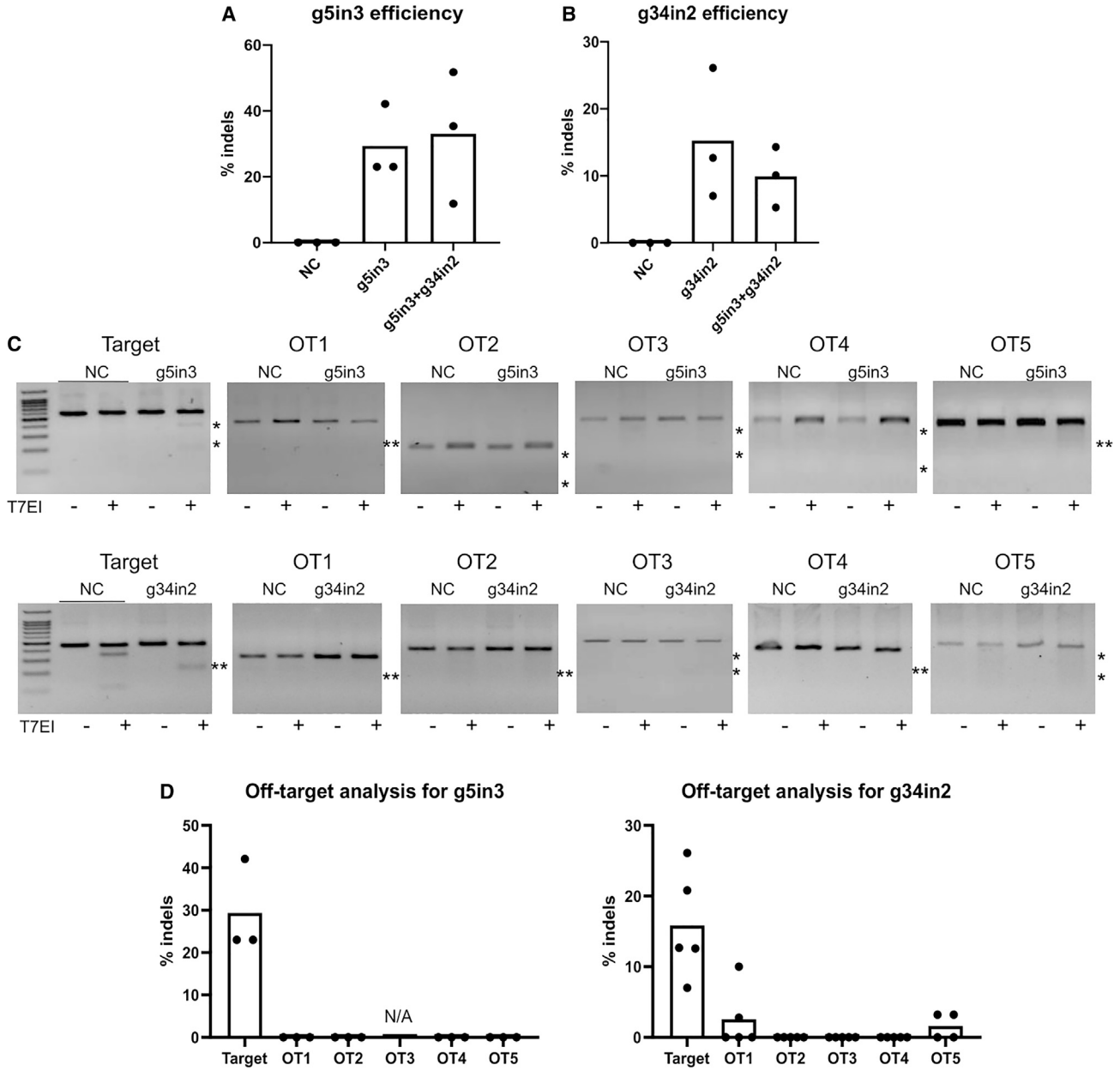

Figure 3. On-target and off-target (OT) activity of guides in primary myoblasts

(A) On-target activity of the g5in3 guide calculated by TIDE analysis in cell culture transduced by a single vector and double-cut editing system. See also Figure S3B. (B) On-target activity of the g34in2 guide calculated by TIDE analysis in cell culture transduced with a single vector and double-cut editing system. See also Figure S3C. (C) T7EI assay for on-target and top 5 predicted OT sites for g5in3 (top panel) and g34in2 (bottom panel). Asterisks indicate the expected cleavage bands. (D) OT activity of g5in3 and g34in2 guides calculated by TIDE analysis. The g5in3 OT3-surrounding sequence is highly repetitive and does not allow us to perform TIDE analysis (marked as N/A on the chart).

Next, we analyzed the top 5 off-target (OT) sites predicted for each guide in the genomic DNA (Table S2). No indel formation in the OT sites was detected by the T7EI assay (Figure 3C). TIDE analysis revealed insertion for g34in2 OT1 in two of five replicas at 2.8% and 10% and for g34in2 OT5 in two replicas at 3.2% (Figure 3D). The OT1 site is within the intron of the predicted lncRNA gene and within the intron of the overlapping non-processed pseudogene. The OT1 and OT5 sites are several dozen kilobases from the nearest annotated protein-coding genes. Given the low percentage of editing, formation of indels in this area is unlikely to cause unwanted

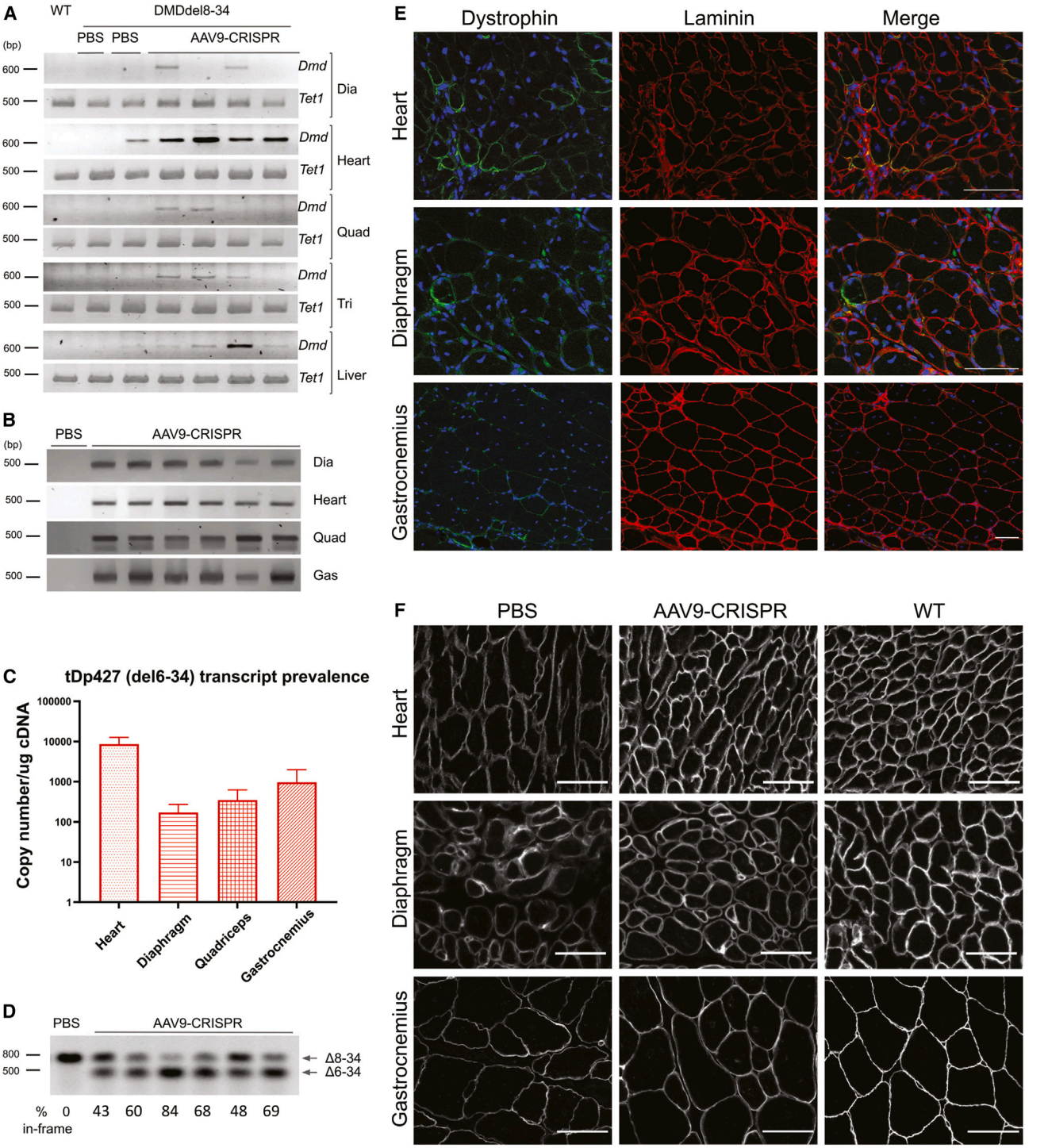

Figure 4. *In vivo* genome editing efficiency following systemic delivery of the editing complex to DMDdel8–34 mice

A mix of AAV9 encoding genome editing complexes was administered via intravenous injections (2E+14 VG/kg of each). Analysis was performed at week 12 post treatment. (A) Amplicons of the genomic DNA indicating removal of the exon 6–7 fragment in the *Dmd* gene (623 bp). *Tet1*, amplicons of the control gene (460 bp). (B) RT-PCR analysis to identify the presence of the shortened dystrophin transcripts (512 bp). Dia, diaphragm; Quad, quadriceps; Tri, triceps; Gas, gastrocnemius. (C) Comparison of shortened *Dmd* transcripts levels in different organs with normalization on the *RPL13*, *Csnk2a2*, and *Ap3d1* genes. Transcript copy number is shown per mkg of cDNA. Data are

(legend continued on next page)

reactions to the CRISPR-Cas9 complex action in mice. However, these results further highlight the need for careful testing of the potential OT effects of genome editing systems designed for use in humans.

Systemic delivery of AAV-CRISPR improved cardiorespiratory function

The potential of the guide combination 5in3+34in2 was further tested *in vivo* following systemic AAV9-mediated delivery. Eight-week-old DMDdel8-34 mice were injected with AAV9-5in3 and -34in2 (2E+14 VG/kg of each) into the retroorbital sinus, and genome editing was assessed 12 weeks post injection. The targeted deletion in the *DMD* genomic sequence was detected by PCR in muscular tissues and the liver (Figure 4A). Accordingly, transcripts of the corrected dystrophin were present in the heart, diaphragm, and skeletal muscles of all analyzed animals (Figure 4B). A quantitative analysis highlighted the abundance of the shortened transcript in the heart (Figure 4C), which correlates well with AAV9 biodistribution. The prevalence of the corrected transcript in the heart varied between animals, with an average value of 62% (Figure 4D). Overall, the editing efficiency of the mutant dystrophin in the heart following systemic delivery of Cas9 and guides was comparable with the efficiency observed after local injections into the TA muscle (Figures 4C and S2A).

Next, we studied the presence of the dystrophin protein in myofibers and restoration of the DAGC components on the sarcolemma in CRISPR-Cas9-treated DMDdel8–34 mice. Dystrophin-specific immunostaining (Figure 4E) followed by quantitative analysis (Figure S4A) determined an average of 60% positive fibers in the heart, 35% in the diaphragm, and 28% in the gastrocnemius muscle. However, the signal intensity of the sarcolemmal dystrophin in the heart samples was much weaker compared with wild-type animals (Figure S4B). Synthesis of the corrected dystrophin in myofibers also led to partial restoration of the DAGC on the sarcolemma, as evidenced by immunostaining for α-sarcoglycan (Figures 4F and S4C) and α-syntrophin (Figure S4D) and western blot analysis of β-dystroglycan expression (Figures S4E and S4F). In the heart, an increase in the sarcolemmal localization of α-sarcoglycan was significant in AAV9-CRISPR-treated animals (Figures 4F and S4C). In the diaphragm and skeletal muscles, we documented only moderate changes in the staining of DAGC components (Figures 4F and S4D–S4F).

To estimate the therapeutic effect of the CRISPR-Cas9-mediated correction of the *DMD*, we analyzed the recovery of muscle function in treated DMDdel8–34 mice. Cardiorespiratory function was measured *ex vivo* in isolated heart and diaphragm muscles. In genome-edited animals, the blood pressure elevation induced by dobutamine was similar to that in wild-type animals and reached 30% in contrast to 15% in the saline-treated group (Figure 5A). Repeated diaphragm contractions resulted in a strength deficit of up to 70% of the DMDdel8–34 muscle. Genome editing reduced this index to 40%–50%, characteristic of wild-type animals (Figure 5B). The specific force of isolated skeletal muscle did not improve significantly after AAV9-CRISPR injections (Figure 5C). Genome-edited DMDdel8–34 mice also showed only slight recovery in the in-life functional tests. Although mice tended to improve their performance in the hanging wire and rotarod tests 4 weeks post treatment, their motor skills declined to those of nontreated controls at later time points (Figures 5D and S5A). Grip strength (Figure 5E) and weight lifting (Figure S5B) did not differ significantly between the genome-edited and saline-treated groups. 12 weeks post treatment, serum CK levels remained high in AAV9-CRISPR-treated animals, indicating progressive muscle damage (Figure 5F). Treated DMDdel8–34 mice did not show a significant difference from nontreated mice in body weight dynamics and functional improvement of cognitive-behavioral characteristics analyzed in the elevated plus maze and object recognition tests (Figures S5C–S5E).

Finally, we evaluated the treatment outcome on the histological manifestations in the hearts, diaphragms, and skeletal muscles of DMDdel8–34 mice (Figure S6A). Quantitative analysis of muscle cross-sections did not indicate a reduction in central nucleus count (Figure S6B). Interestingly, we found that systemic AAV-CRISPR delivery differently affects the distribution of the fiber sizes in the diaphragm and skeletal muscle. In the diaphragm, the diameter of myofibrils normalized and approached the size of wild-type muscle (Figure 5G). In contrast, the fraction of small fibers (diameter of 10–20 μm) increased in the TA muscle, which indicates progressing damage and regeneration (Figure 5H). The level of hydroxyproline in tissue is a quantitative indicator reflecting fibrosis and collagen content.[28] In the diaphragm of AAV-CRISPR-Cas9-treated mice, the hydroxyproline level decreased, but the differences from the control group were insignificant (Figure S6C). Muscle inflammation, as measured by infiltrating CD68+ cells, was not reduced significantly in treated DMDdel8–34 mice compared with the nontreated counterparts (Figure S6D).

In summary, we found definite signs of functional and histological improvement in DMDdel8–34 mice after systemic delivery of the CRISPR-Cas9 genome editing complex. In cardiac muscle, restoration of dystrophin caused normalization of the dobutamine-induced response and an increase in presentation of the α-sarcoglycan component of the DAGC on the plasma membrane. In the diaphragm, we found a decrease in force deficit after repeated contractions and a rightshift in the distribution of fiber sizes. Despite this, skeletal muscle did not show any positive significant changes and did not worsen, as demonstrated by the hanging wire test and fiber size distribution.

presented as the mean + SD. n = 6–10 animals per group. (D) RT-PCR results with primers detecting native (822 bp) and shortened *Dmd* transcripts (530 bp) in heart samples. Relative quantities of transcripts with restored reading frames are indicated. (E) Immunofluorescence analysis of skeletal muscle, heart, and Dia cryosections. Dystrophin is green (Ab15277), laminin is red (Ab11576), and nuclei are counterstained blue. Scale bars, 50 μm. See also Figures S4A and S4B. (F) DAGC component α-sarcoglycan staining (ab189254). Scale bars, 50 μm. See also Figure S4C. Representative images from three independent experiments are shown.

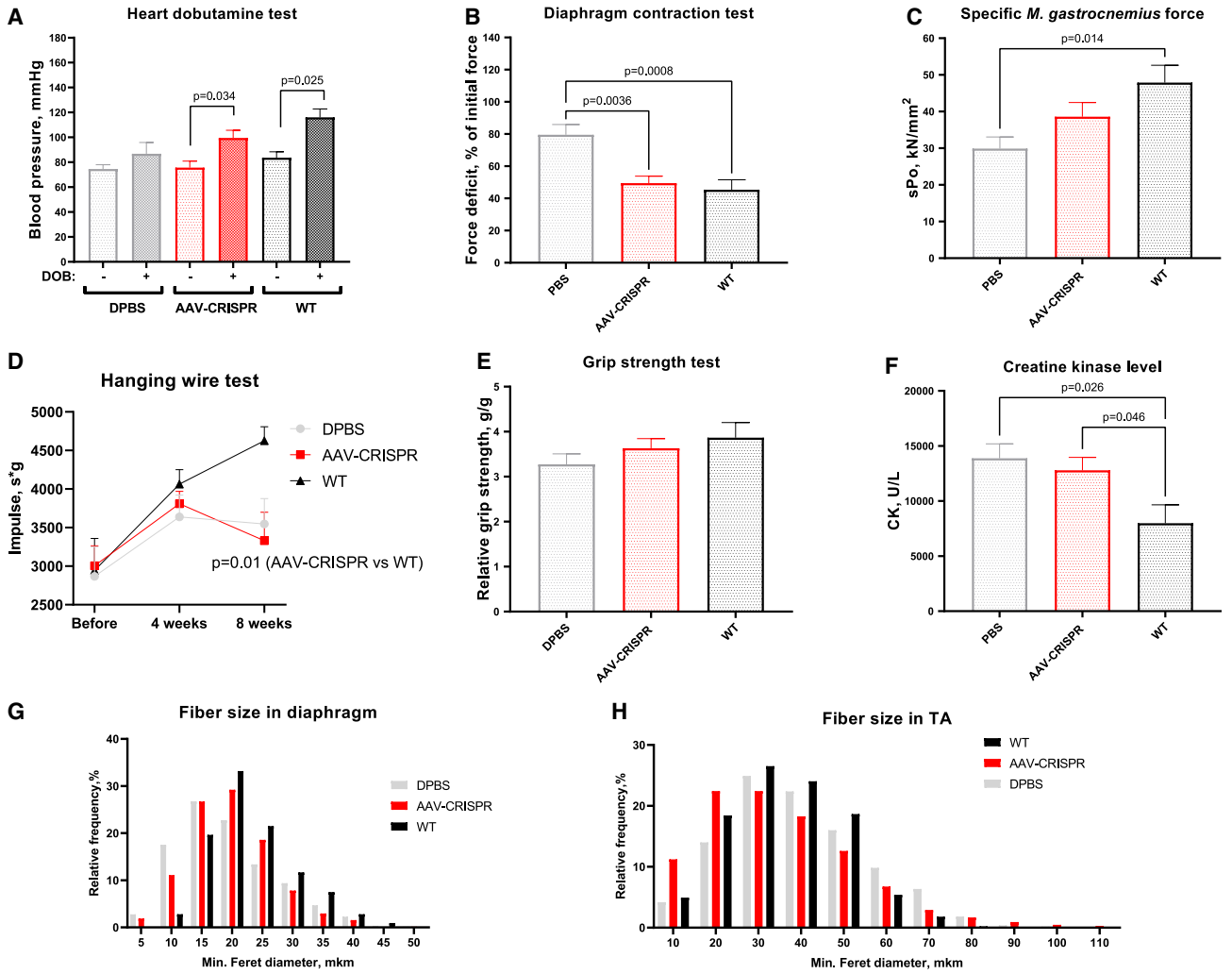

Figure 5. The physiological outcome of *in vivo* genome editing in DMDdel8–34 mice

Shown are results of functional, biochemical, and histopathological analyses 12 weeks post systemic administration of AAV-CRISPR (2E+14 VG/kg of each AAV9-encoding genome editing complex). (A) Blood pressure in the carotid artery after dobutamine (DOB) probe, describing heart function. (B) Dia force deficit after repeated contractions to assess the recovery of muscle strength. (C) Specific force of skeletal muscle *in situ*, showing contractile muscle properties. (D) Hanging wire test. (E) Grip strength test. Additional tests are presented in Figure S5. (F) CK level in blood serum, reflecting the degree of muscle damage. The high CK in the WT group is probably of non-muscular origin. (G) Fiber size distribution in the TA muscle. (H) Fiber size distribution in the Dia. See also Figure S6. Data were obtained in 3 independent experiments. Data are presented as the mean + SD. N = 10 mice in each group.

Genomic editing results in truncated mDp427 expression, albeit at a low level

To demonstrate the production of CRISPR-Cas9-corrected dystrophin, we probed muscle samples with dystrophin-specific antibodies following local and systemic delivery of the editing complex (Figure 6A). Translation of the *DmdDel6-34* transcript should result in the truncated dystrophin (designated tDp427) lacking the actin-binding calponin homology domain 2 (CH2) within the N-ABD and a portion of the rod domain (Figure 6A). We created a plasmid with CMV-driven expression of the dystrophin coding sequence without exons 6–34 as in tDp427. Western blot analysis of plasmid transfection into HEK293T cells revealed successful production of the shortened dystrophin with an estimated molecular weight of 230 kDa (Figure 6B). Systemic delivery of AAV-CRISPR did not yield a detectable level of a 230-kDa protein product in the heart, diaphragm, or skeletal muscle (Figure S7), in concordance with the modest functional recovery of DMDdel8-34 mice (Figures 5 and S5). Following intramuscular injections, a protein band corresponding to tDp427 appeared in TA lysates of CRISPR-Cas9-edited mice (Figure 6C). In addition, treated and control samples stained positive for dystrophin isoforms Dp140 and Dp116. The quantitative analysis estimated the expression level of tDp427 to be 0.6%–4.8% from the amount of full-length dystrophin (Dp427) in wild-type animals (Figure 6D).

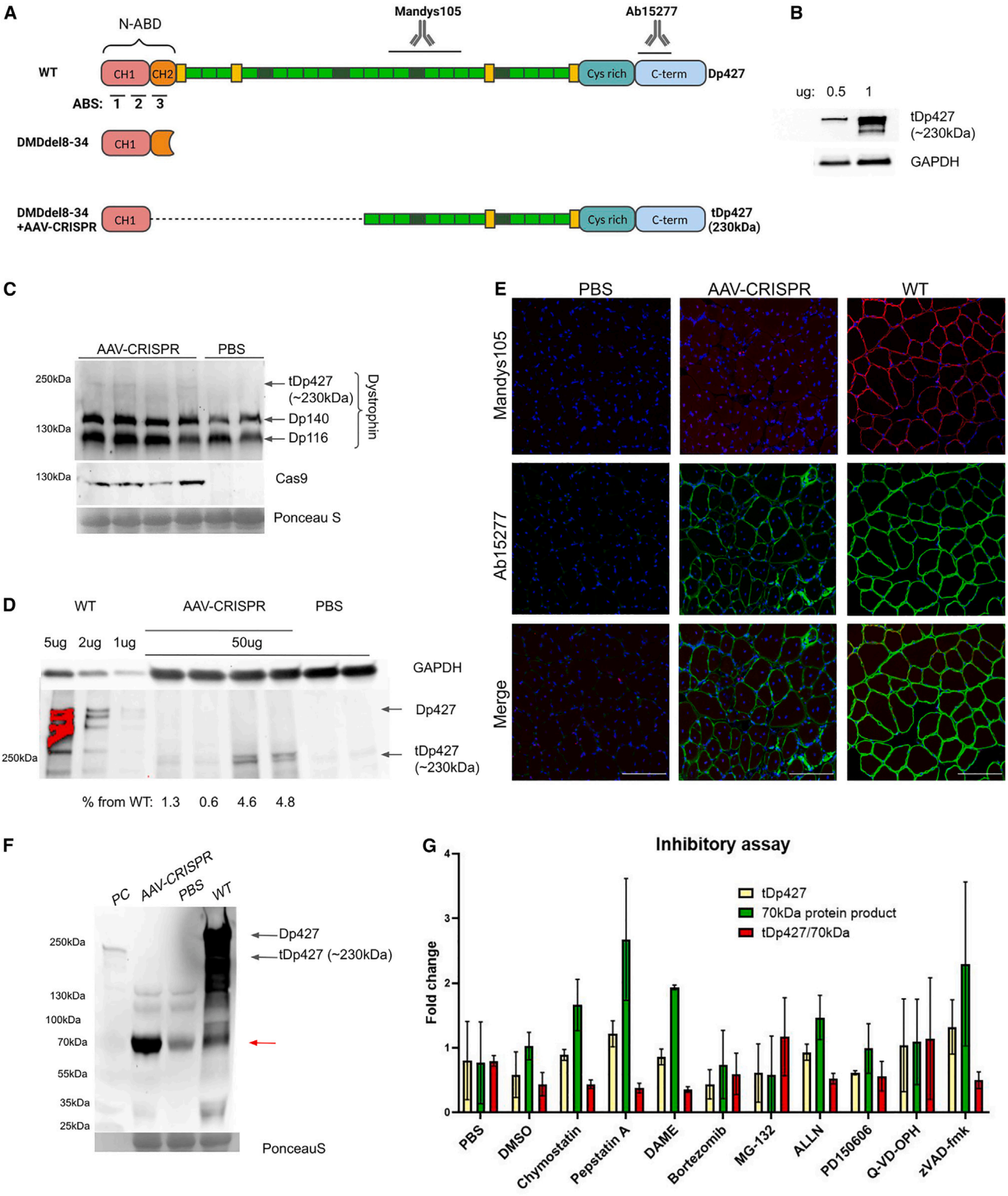

Figure 6. Truncated dystrophin expression in the skeletal muscles of DMDdel8–34 mice after intramuscular injection of the genome editing complex

(A) Schematic of dystrophin Dp427m isoforms and epitopes recognized by dystrophin antibodies. (B) Detection of tDp427 protein in HEK293T cells after transfection with the control plasmid pDmdDdel6-34 encoding *Dmd* cDNA with deletion of exons 6–34 under the CMV promoter. The quantity of plasmid used for transfection is shown. Loading

(legend continued on next page)

Mandys105 antibody, specific to the distal portion of the rod domain preserved in tDp427 (Figure 6A), failed to detect a low amount of the truncated protein in the muscle sections (Figure 6E). In contrast, an antibody to the CT domain of dystrophin (Ab15277) recognized antigen on the sarcolemma of TA muscle fibers (Figures 6A and 6E). The same antibody used for western blotting detected an abundant band with an approximate molecular weight of 70 kDa in CRISPR-Cas9-treated muscles (Figure 6F). We speculated that sarcolemma staining with Ab15277 antibody represents an abundant 70-kDa dystrophin product rather than the 230-kDa truncated protein detected in trace amounts by western blotting.

The low amount of truncated tDp427 protein (Figures 6C and 6D) was inadequate compared with the expression level of the corrected transcripts after AAV9-5in3 and -34in2 treatment (Figure 2B). We hypothesized that the CRISPR-Cas9-generated 230-kDa dystrophin was unstable and subject to proteolysis. Similarly, the reduced expression (10% of the wild-type) of the truncated dystrophin was observed in rats carrying the in-frame deletion in the 5′ region of *Dmd*, and enhanced proteasomal degradation was suspected.[29] To identify the degradation pathway, we tested protease inhibitors specific to lysosomal cathepsins (chymostatin, pepstatin A, DAME), the proteasome (bortezomib, MG-132), calcium-activated cytosolic calpains (ALLN, PD150606), and caspases triggering apoptosis (Q-VD-OPH, zVAD-fmk). We administered the AAV-CRISPR into the TA of DMDdel8–34 mice, and before sample collection, animals were treated for 24 h with the protease inhibitors via intraperitoneal injections. We did not capture significant inhibitor-related recovery of tDp427 because of the high variability of the truncated protein synthesis between individual animals (Figure 6G). This technical limitation does not allow us to identify proteolytic pathways involved in tDp427 degradation; however, the data are insufficient to reject the hypothesis about tDp427 proteolysis in muscle tissues.

Another speculation is that the abundant 70-kDa protein from CRISPR-Cas9-edited samples (Figure 6F) is the product of tDp427 proteolytic cleavage. We examined the levels of the 70-kDa protein in conjunction with tDp427 within each mouse in control and inhibitor-treated groups (Figure 6G). None of the tested inhibitors increased the ratio of tDp427 to the 70-kDa product, as one would expect if the shorter protein resulted from proteolysis.

We conclude that truncated 230-kDa dystrophin is produced in muscle tissue upon AAV-CRISPR genome editing, but the reason for the low expression remains undetermined. We also report the presence on the sarcolemma of an abundant 70-kDa protein that does not originate from proteolytic digestion of the corrected dystrophin.

Dystrophin isoform Dp71 is upregulated in CRISPR-Cas9-treated skeletal muscles

The 70-kDa protein detected by the dystrophin-specific antibody in edited muscles could potentially be Dp71, a shorter dystrophin isoform (Figure 7A). Dp71 protein with a molecular weight of 70.4 kDa is ubiquitously expressed from the internal promoter in neuronal tissue.[30] It has been described previously that the Dp71 isoform is expressed in myocytes but absent in mature muscle cells.[31] However, recent findings revealed the presence of Dp71 in skeletal muscle.[32] We used 5′-RACE analysis to estimate the abundance of Dp71 among all dystrophin transcripts in the muscles of CRISPR-Cas9-treated DMDdel8–34 mice (Figure 7B). In the muscles of wild-type mice, Dp427m is expectedly the most represented. In the absence of Dp427m, the isoform balance drastically changes, and the Dp71 transcript becomes overrepresented (10/10) in the muscles of DMDdel8–34 mice injected with AAV-CRISPR or left untreated. Notably, no previously uncharacterized transcripts encoding dystrophin with a molecular weight of approximately 70 kDa were found, except for Dp71.

Unlike the Dp427 transcript, Dp71 is susceptible to alternative splicing. Over 10 Dp71 splice variants in normal and malignant tissues or model systems have been described.[30,33,34] Some isoforms are common in undifferentiated satellite cells rather than in myotubes,[35,36] and specific amino acids in different splice forms can regulate protein localization.[37] To specify splice variants upregulated in CRISPR-Cas9-treated DMDdel8–34 mice, we amplified full-length Dp71 cDNA (~2 kb; Figure S8A) and identified exon content by Sanger sequencing. We discovered a Dp71d splicing variant with exons ranging from G1 to 79 in all of the groups studied (Figure 7A). Approximately 30% of the transcripts were represented by the Dp71f isoform lacking exon 78 and with an alternative C terminus (Figures 7A and 7C). A small percentage of the transcripts also lacked exon 71 (Figure 7C). Interestingly, exons 71 and 78 were not absent simultaneously, as revealed by Sanger sequencing of individual clones. To identify the splice variant that translates to abundant 70-kDa protein, we used two antibodies discriminating different C termini of dystrophin. Ab15277 recognizes Dp71d and Dp71f, while NCL-Dys2 is specific to the exon 78-encoded peptide and recognizes only Dp71d (Figure 7A). Immunofluorescence analysis displayed the absence of amino acids encoded by exon 78, indicating that the

control, GAPDH. (C) Detection of tDp427 and Cas9 proteins in total TA muscle lysates 2 weeks after genome editing. The estimated molecular weight of dystrophin after reading frame restoration is 230 kDa. Loading control, Ponceau S. (D) Estimation of tDp427 quantity in treated muscles in comparison with full-length Dp427 in wild-type muscles. Loading control, GAPDH. The amount of protein lysate (micrograms) applied to each well is indicated at the bottom. Band saturation is shown in red. (E) Immunofluorescence analysis of frozen muscle cross-sections with antibodies to the dystrophin rod domain (Mandys105, red) and C terminus (Ab15277, green). Nuclei were counterstained blue. Scale bars, 20 μm. (F) Western blot analysis of TA muscle lysates with antibodies against the C terminus of dystrophin on the full membrane. Overexpression of the 70 kDa protein (red arrow) was found in AAV-CRISPR-treated muscle, along with equal expression of the Dp116 and Dp140 dystrophin isoforms. PC, HEK293T lysate after transfection with pDmdDel6–34; loading control, Ponceau S. (G) Effect of protease inhibitors on accumulation of tDp427 and 70-kDa proteins in the muscles of CRISPR-Cas9-treated mice. Quantification of the western blots is shown. Data are presented as the mean ± SD. n = 4 per group.

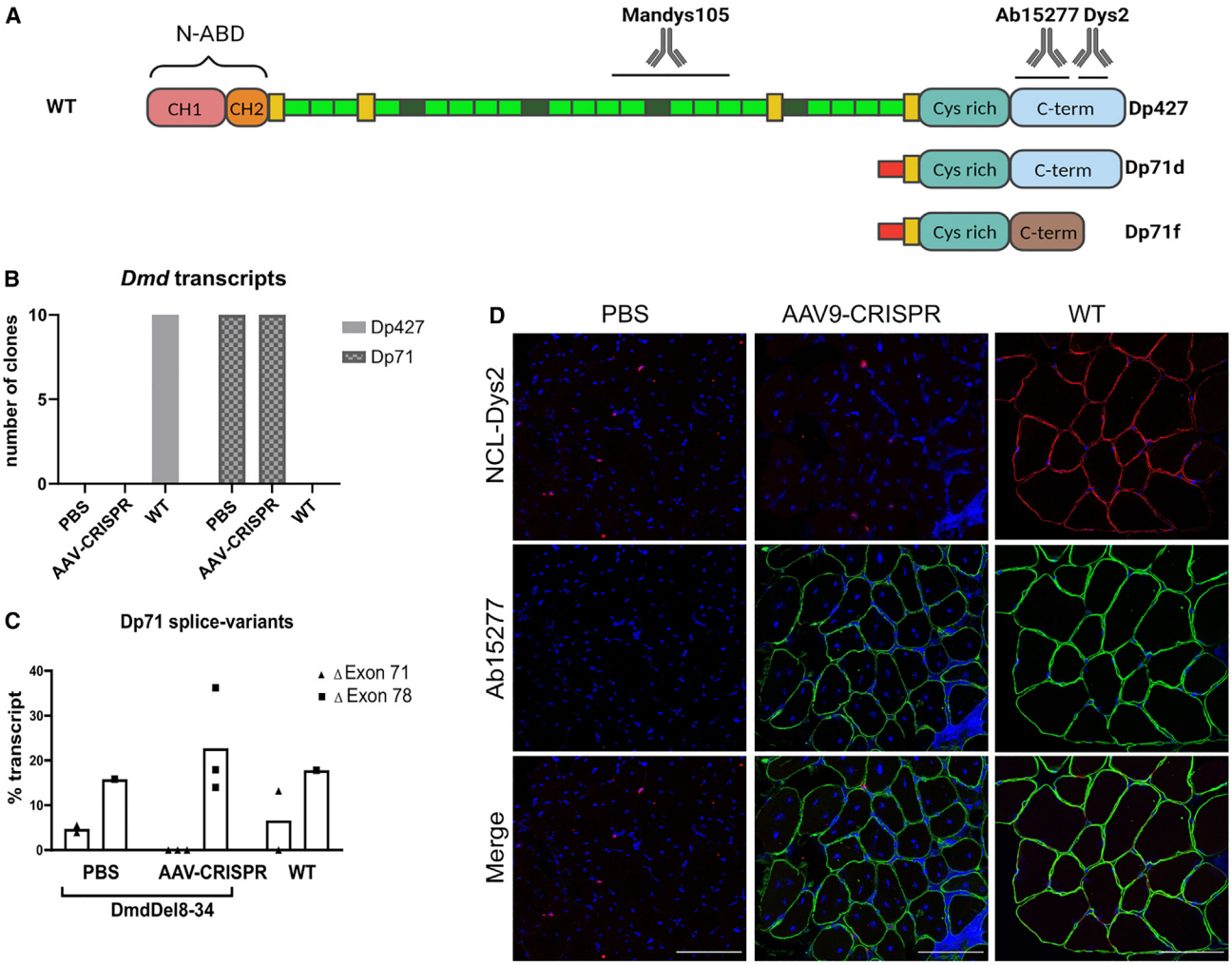

Figure 7. Dp71f protein is upregulated and localizes to the sarcolemma in muscles of genome-edited DMDdel8–34 mice

(A) Schematic of Dp427m and Dp71 isoforms with epitopes of antibodies to the C terminus of dystrophin. (B) Prevalence of *Dmd* transcripts in TA muscle according to 5'-RACE analysis. 10 clones were analyzed per mouse per group. (C) Relative abundance of *Dp71* splice variants in mouse muscles. Using specific primers for unique exon G1 and exon 79 (Table S3), the PCR product (~2 kb) corresponding to the full-length Dp71 cDNA was amplified (Figure S8A). Sanger sequencing results were analyzed using DECODR v.3. (D) Immunofluorescence analysis of frozen TA muscle cross-sections with antibodies against the dystrophin C terminus (NCL-Dys2, red; Ab15277, green). Nuclei were counterstained blue. Scale bars, 20 μm.

protein raised on the sarcolemma is Dp71f (Figure 7D). At the same time, NCL-Dys2 antibodies successfully recognized tDp427 protein translated from the control plasmid (Figure S8B). The CR and CT domains of Dp71f are nearly identical to the Dp427m sequence (Figure 7A), and Dp71f can bind the DAGC components. Indeed, we found increased α-sarcoglycan presentation on sarcolemma of AAV-CRISPR-injected TA muscles (Figure S8C).

In several mice administered AAV-CRISPR via intramuscular injections, we identified a shorter 600-bp PCR product in addition to 2 kb of full-length Dp71 cDNA (Figure S8A). This product represented a previously undescribed Dp71 isoform with spliced-out exons 63–74, where exon G1 was directly linked to exon 75 of the *Dmd* gene (Figure S8D). In this case, the reading frame was not shifted, retaining translation of the protein with the C terminus characteristic of Dp71d and a molecular weight of 20 kDa.

CRISPR-Cas9 genome editing, but not PMO-induced exon skipping, upregulates Dp71f

To define the mechanism of Dp71f protein upregulation, we compared its transcript levels by qRT-PCR analysis throughout animal groups. Surprisingly, we did not find an elevation in Dp71 transcript levels in genome-edited or saline-treated DMDdel8–34 mouse muscles compared with the wild-type control (Figure 8A). We speculate that Dp71 overrepresentation is due to regulation at the post-transcriptional level. The finding that the protein turnover rate,

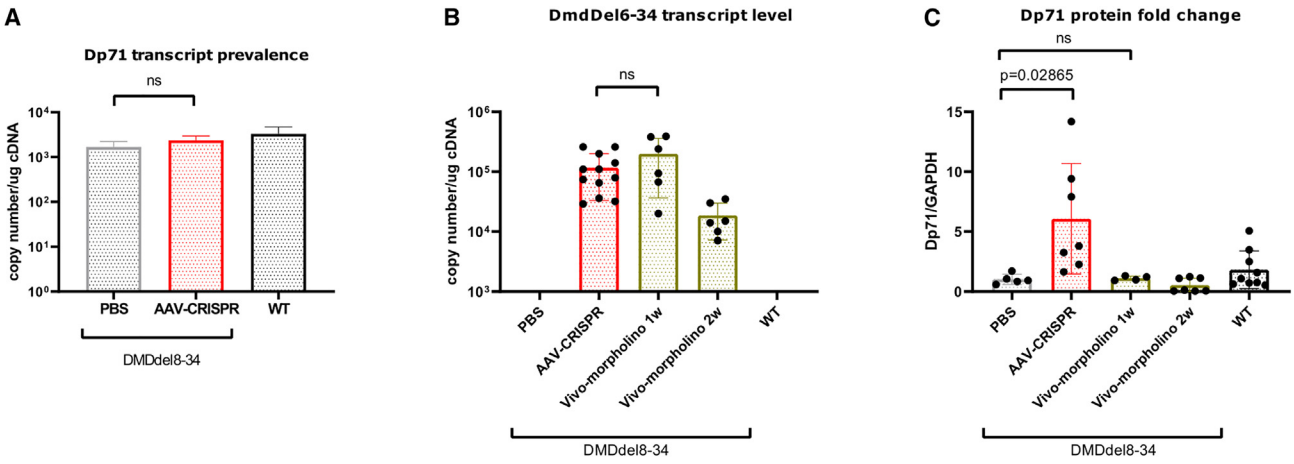

Figure 8. Dp427 and Dp71 expression following intramuscular injections of genome-editing versus exon-skipping instruments

(A) Absolute *Dp71* transcript level in skeletal muscle, determined by qRT-PCR with normalization on the *RPL13*, *Csnk2a2*, and *Ap3d1* genes. Transcript copy number is shown per microgram of cDNA. Data are presented as the mean + SD. N = 4 per group. (B) Absolute *tDp427* (*DmdDel6-34*) transcript level in skeletal muscle after single injection of AAV-CRISPR (2 weeks) versus PMO (1 and 2 weeks post injection) with normalization on the *RPL13*, *Csnk2a2*, and *Ap3d1* genes. Transcript copy number is shown per mkg of cDNA. Data are presented as the mean ± SD. (C) Relative Dp71 protein level in skeletal muscle according to western blotting, normalized to the DMDdel8–34 group injected with PBS. Loading control, GAPDH. Data are presented as the mean ± SD. See also Figure S9.

rather than transcriptional control, tightly controls the amount of Dp71 in neuronal cells provides additional evidence in favor of this theory.[38]

Finally, we explored whether Dp71f upregulation is induced by the genome editing procedure or by the presence of the corrected transcript with unnatural exon composition. To verify whether *DmdDel6-34* mRNA can directly upregulate Dp71f, we induced formation of the transcript by a CRISPR-Cas9-independent approach, using vivo-PMO for exon skipping. DMDdel8–34 mice were injected intramuscularly with AAV-CRISPR or vivo-PMO, previously optimized for skipping exons 6 and 7.[39] One and two weeks post injection, muscles were collected for RT-PCR and western blot analysis. Comparable expression of the *DmdDel6-34* transcript in treated muscles was demonstrated for AAV-CRISPR and vivo-PMO (Figure 8B). In line with our previous results, the genome editing and PMO-induced exon skipping did not produce detectable levels of tDp427 dystrophin (230 kDa) in treated muscles (Figure S9). Importantly, an increased Dp71f level was detected only following CRISPR-Cas9-mediated genome editing but not after exon skipping driven by vivo-PMO (Figures 8C and S9). We conclude that *DmdDel6-34* mRNA does not inherently increase Dp71 presentation. Dp71 upregulation appears to arise from the CRISPR-Cas9-mediated genome editing procedure, although the mechanism is unknown.

DISCUSSION

For over a decade, researchers have tried to harness CRISPR-Cas9 genome editing to correct out-of-frame deletions in the *DMD* gene and develop a cure for DMD.[10–12] The location of the mutation in the gene affects the functionality of the shortened dystrophin produced after CRISPR-Cas9-mediated restoration of the reading frame. Multiple animal studies report successful restoration of the reading frame within the rod domain, which contains the mutation hotspot in exons 45–55.[14,17,40–42] The resulting dystrophin retains functionality because of the redundancy of SR. In contrast, tackling the mutations disturbing the N-ABD (hotspot in exons 2–20) appears to be challenging because truncation of the actin-binding regions in dystrophin may interfere with protein stability and functionality.[43–45]

In the present study, we applied the AAV-CRISPR double-cut technology to restore dystrophin with a unique patient-specific deletion of exons 8–34 (Figure 6A). Genome editing tools were delivered into DMDdel8–34 mice[23] via intramuscular and intravenous injections. We achieved successful excision of exons 6 and 7 from the *Dmd* gene (Figures 4A and S1) and expression of the corrected transcripts *in vivo* (Figures 4B and 4D). We also detected production of the truncated 230-kDa dystrophin (tDp427), albeit in low quantities. Nonetheless, the amount of the truncated dystrophin after local injections was sufficient to promote recovery of skeletal muscle in DMDdel8–34 mice (Figures 2D–2F). CRISPR–Cas9 systemic delivery improved the performance of the heart and diaphragm muscles (Figures 5A and 5B). Our data indicate at least partial functionality of dystrophin without exon 6–34 sequences encompassing the CH2 subdomain in the N-ABD and the 5′ terminal portion of the rod domain (Figure 6A). We speculate that truncated dystrophin in our study retains actin-binding properties because of the intact CH1 subdomain.

Several studies have addressed the functional capacity of the truncated dystrophins with in-frame deletions in the N-ABD. Banks et al.[46] demonstrated that AAV-delivered, highly expressed microdystrophins lacking actin-binding sequences (ABS2, ABS3, or ABS3 alone) have a reduced ability to promote muscle recovery compared with microdystrophin DeltaR4-R23/DeltaCT with an intact N-ABD

domain.[46] In contrast, two independent studies claimed generation of functional dystrophin without ABS3 located in the CH2 subdomain.[45,47] Kyrychenko et al.[45] performed CRISPR-Cas9-mediated removal of exons 3–9 or 6–9 in the DMD model of induced pluripotent stem cell (iPSC)-derived cardiomyocytes. Echigoya et al.[47] induced simultaneous skipping of exons 6 and 8 with subsequent splicing of exons 5–9 or 10 in a canine model of DMD. In both studies, the truncated dystrophin without CH2 was effectively expressed and functionally active. Interestingly, excision of exons 3–9 was preferable for protein function in cardiomyocytes over exon 6–9 deletion. There is also a reported case of a patient with exon 3–9 deletion and an asymptomatic phenotype.[48] These observations strengthen our assumption that 230-kDa dystrophin lacking a subportion of the N-ABD is potent in muscle tissues, although additional functional analysis regarding tDp427 is required.

The low presentation of tDp427 in muscles observed in our studies (Figures 4E, 6C, 6D, and S4B) can reflect the inefficiency of CRISPR-Cas9-mediated multi-exon excision. Indeed, there are reports demonstrating limited efficiency of the double-cut strategy compared with reframing or splice site disruption induced by single-cut editing systems.[49,50] Some options to increase genome editing efficiency include modulation of the Cas9-to-gRNA ratio,[15] utilizing a self-complementary AAV (scAAV) with a higher processing rate and better episomal persistence,[51] and optimizing targeted delivery of the editing complexes with novel myotropic AAV serotypes.[52]

Several studies report that dystrophins with mutations in the N-ABD have reduced stability and are subject to proteolysis,[43–45] which could also explain abnormally low presentation of tDp427 in our studies. In one of the studies, CRISPR-Cas9 genome editing was applied to delete *DMD* exons 7–11 in iPSC-derived cardiomyocytes.[45] Treating cardiomyocytes with the proteasome inhibitor MG-132 increased levels of the truncated protein, confirming proteasomal degradation of the dystrophin lacking exons 7–11. The importance of N-ABD integrity for protein stability and presentation in muscle tissues is further supported by the patient data. BMD patients with in-frame mutations in the N-ABD demonstrate more severe phenotypes compared with typical disease manifestations (Table S4). The severe phenotype correlates with the low presentation of dystrophin with a disrupted N-ABD in the patients' muscles. In our work, we failed to identify the protease-dependent pathways involved in degradation of the truncated dystrophin; nevertheless, instability of the tDp427 protein appears likely. We speculate that the conformation of the truncated protein differs substantially from the normal dystrophin. In the full-length dystrophin, the N-ABD is connected to SR1 through H1, providing flexibility to the whole molecule. The tDp427 protein lacks the CH2 subdomain and the proximal portion of the rod domains with H1 and H2 (Figure 6A). The direct connection of the CH1 subdomain with incomplete SR12 can account for tDp427 protein instability and lead to its degradation.

Another finding of our study is upregulation in the CRISPR-Cas9-treated mice of the dystrophin Dp71f, a 70-kDa isoform (Figures 6F and 7). This protein contains the same CR and CT domains as Dp427m, except for the last amino acids of the CT domain (Figure 7A). Presentation of the Dp71 isoform in mature skeletal cells leads to restoration of the DAGC on the sarcolemma.[53,54] However, Dp71 expression in muscle can also cause muscle damage similar to DMD and heart dysfunction.[53,55] The ability to bind the DAGC component on the sarcolemma without actin-binding capacity made Dp71 a dominant-negative competitor of Dp427m dystrophin.[56] For instance, Dp71 upregulation coincided with a severe disease course in canine models of DMD, with inversions of the *Dmd* gene disrupting intron 29[57] or 20[58] or with splice-site mutation in intron 6.[54] Another study described an in-frame deletion of exon 3–16 in rats, which resulted in appearance of a 70-kDa dystrophin product designated DpX.[29] The authors found reduced expression of truncated dystrophin and explained this by protein degradation with formation of DpX. Unexpectedly, truncated dystrophin expression did not prevent muscular dystrophy, and animals differed significantly from wild-type counterparts.[29] Dp71 upregulation was also detected *in vitro* in an iPSC-derived model of DMD lacking exon 52.[59] The source of Dp71 upregulation remains unknown and requires careful investigation. In DMDdel8–34 mice, we show that the abundant 70-kDa protein is not a degradation product of the corrected dystrophin (Figure 6G). Moreover, we find that CRISPR-Cas9 genome editing, but not exon skipping, accomplished through PMO increases Dp71 levels (Figures 8B and 8C).

To summarize, our results and independent studies unravel intricacies regarding CRISPR-Cas9 genome editing for DMD with out-of-frame deletions in the exon 2–20 hotspot. Besides the efficiency of the CRISPR-Cas9 technology, functional recovery depends on the functionality and stability of the corrected dystrophin with the truncated N-ABD. CRISPR-Cas9-correction can upregulate Dp71, leading to Dp71-associated muscle pathology. The described limitations further complicate development of CRISPR-Cas9-based therapeutic approaches for mutations within the 5′ hotspot. Therefore, gene replacement therapies using microdystrophins remain the most feasible regardless of the mutation type. Patients with N-ABD mutations could also benefit from the CRISPR-Cas9-based technologies for restoration of the full-length dystrophin, such as homology-independent targeted insertion (HITI) or related approaches.[19]

MATERIALS AND METHODS

Ethics

All animal procedures were performed following the requirements of Directive 2010/63/EU, the European Union (EU) legislation "on the protection of animals used for scientific purposes." Experiments were approved by the local animal care and ethics committees of the Institute of Gene Biology and Belgorod State National Research University. The report describing animal experiments was written in accordance with ARRIVE guidelines 2.0.[60]

Plasmid design, molecular cloning, and AAV production

SaCas9 guides were designed for *Dmd* intron 5 and chimeric intron 7/34 in the CHOPCHOP[61] and CRISPR DNA Region Designer

(Horizon Discovery, USA) online tools and selected based on minimal predicted OT activity. Synthetic oligos were obtained from Evrogen (Russia). Complementary oligo strands were annealed, phosphorylated, and cloned into the pX601 plasmid. All guides utilized in this study are reported in Table S1. pX601-AAV-CMV:NLS-SaCas9-NLS-3×HA-bGHpA; U6:BsaI-sgRNA was a gift from Feng Zhang (Addgene plasmid 61591).[62] HEK293T cells were obtained from the American Type Culture Collection (ATCC). The cells used in this work were recently authenticated using short tandem repeat DNA profiling (Gordiz, Russia) and tested for mycoplasma contamination using PCR. HEK293T cells were cultured in high-glucose DMEM (Gibco, USA) supplemented with 10% (v/v) fetal bovine serum (FBS; Biosera Europe, France) and Pen-Strep. Modified px601 plasmids were used in HEK293T triple transfection with the pAAV-RC2/9 (Penn Vector Core, USA) or pAAV-DJ (Cell Biolabs, USA) and pHelper (Agilent, USA) plasmids for recombinant AAV production. The purification procedure has been described previously.[63] Briefly, the cells were lysed with 0.5% (v/v) Triton X-100, 5 μg mL-1 RNAse A, and 10 μg mL-1 DNase A for 1 h at 37°C with shaking. Clarified and concentrated virus suspensions were subjected to ultracentrifugation in a modified version of an iodixanol density step gradient for 1 h at 350,000 × *g* and 18°C. The AAV-containing fraction was dialyzed using a 100-kDa membrane against storage buffer (PBS, 350 mM NaCl, 0.001% Pluronic F-68), concentrated, and sterilized. The encapsidated VG titer was determined using primers and a fluorescence probe targeting the ITR sequences. The absence of protein impurities in preparations was confirmed by silver staining.

To construct a positive control plasmid, the 5′ part of murine dystrophin cDNA from exons 1–5 and the 3′ part from exons 35–79 were amplified from skeletal muscle samples of wild-type mice using primers sp1F and e1-5R and e35-79F and e35-79R, respectively (Table S3). To insert the truncated *Dmd* open reading frame (ORF) instead of GFP, the pEGFP-C1 (Clontech, USA) vector was linearized with the pC1F and pC1R primers. Plasmid assembly was performed using the NEBuilder HiFi DNA Assembly Kit (New England Biolabs, E5520S) with the overlapping primers sp1f, sp2f, and sp3f (Table S3). The resulting construct was designated pDmdDel6–34.

The antisense oligonucleotides used in the current study were designed to exonic splice enhancer within *Dmd* exon 6 (+62+86), mB002 5′-GTTGACTGTCGAACCCAGCTCAGA-3′, and exon 7 splicing donor (+05–19), mB009 5′-CCAACCTTCAGGATCAAGAAGTTT-3′. PMOs were synthesized and covalently conjugated to a nonpeptide-based transporter (vivo-PMO, Gene Tools).[64]

Cell culture and sgRNA screening

To establish primary cell culture, skeletal muscles from neonatal male DMDdel8–34 mice were microdissected into cubes using sterile blades. The chopped tissue was treated with 100 U/mL collagenase type II (Paneco, II013-2) in serum-free DMEM/Ham's F-12 medium (Paneco) for 30 min at 37°C with frequent agitation. Then, the tissue homogenate was washed twice, filtered through a 70-μm cell strainer, and plated on gelatin-coated 12-well cell culture plates in growth medium (DMEM/Ham's F-12, 10 ng/mL acidic recombinant mouse fibroblast growth factor 1 [FGF-1; F5542, Sigma-Aldrich, USA], 20% FBS, NEAA [Gibco, USA], L-glutamine, and Pen-Strep). On day 4 after plating, the cell growth medium was replaced with differentiation medium (DMEM/F-12) supplemented with 5% horse serum (Gibco), ITS (Paneco), 10 ng/mL FGF-2 basic human recombinant (Paneco), NEAA, L-glutamine, 70 μM CaCl2, and Pen-Strep. Crude viral lysates or purified viral solutions were added to cells immediately after differentiation initiation to a final concentration of 5E+11 VG/mL. The medium was replaced 24 h after transduction and then every other day. Transduction efficiency was monitored using the reporter AAV-DJ encoding GFP. Transfection with pDmdDel6–34 plasmid constructs was performed using Lipofectamine 3000 reagent (Invitrogen, L3000001) according to the manufacturer's recommendations, using 0.5–1 mkg of the plasmid. Cells were collected for analysis on the seventh day after transduction or transfection.

Animal studies

Dystrophin-deficient DMDdel8–34 mice[23] and C57BL6/CBA background mice were bred in a vivarium of IGB RAS. All mice were maintained under a controlled 12-h photoperiod, and water and food were provided *ad libitum*. The male mouse genotype was defined during multiplex PCR with primers surrounding deletion dmd_mus_sgRNA1_fw/sg30rev and control gDNA fragment tet1_vF/R (Table S3). DMDdel8–34 mice were randomized into experimental groups to equally present mice with different disease manifestations. Information about the solutions administered to DMDdel8–34 mice was blinded. Mice were anesthetized with tiletamine hydrochloride/zolazepam hydrochloride mix (50 mg/kg) and xylazine (5 mg/mL) by intraperitoneal injection. For intramuscular delivery, mice received injections of AAV-CRISPR or vivo-morpholinos diluted in 40 μL PBS into each TA muscle (2E+12 VG/muscle and 20 mkg/muscle). Control DMDdel8–34 mice and wild-type mice received injections of PBS. For intravenous delivery, model animals received injections of AAV-CRISPR-Cas9 diluted in 300 μL PBS into the retroorbital venous sinus (150 μL per sinus, 2E+14 VG/kg or 2E+14 VG/kg of body weight). Control DMDdel8–34 mice and wild-type mice received retroorbital injections of PBS (150 μL PBS per sinus). For the inhibitory assay, mice pretreated intramuscularly with AAV-CRISPR received 300 μL of inhibitor solution in PBS during intraperitoneal injections 24 h before muscle collection. The doses of inhibitors were 10 mg/kg chymostatin (Sigma, C7268), pepstatin A (Sigma, P5318), DAME (Bachem, F2220), and ALLN (Sigma, A6185); 0.4 mg/kg bortezomib (Nativa, Boramilan) and Q-VD-OPH (Sigma, SML0063); 1 mg/kg MG-132 (Sigma, C2211) and zVAD-fmk (Calbiochem, 219007); and 3 mg/kg PD150606 (Sigma, D5946).

Mice were euthanized 2 weeks post injection via intramuscular delivery or 12 weeks via intravenous delivery. Tissue samples were collected for gDNA, RNA, protein, histological, and immunofluorescence analysis. Samples for gDNA, RNA, and protein analysis were snap-frozen in liquid nitrogen.

Creatine kinase

Blood was collected from jugular veins before euthanasia. Blood was left for 15 min at room temperature and centrifuged (3,500 × *g* for 10 min at 4°C) to promote clot formation and serum collection. CK activity was determined using the Creatine Kinase Activity Assay Kit (DiaVetTest, Russia) and a NanoPhotometer.

Histopathology

Organs were weighed, fixed in 10% buffered formalin, and embedded in paraffin. Five-micrometer-thick transverse sections were stained with hematoxylin and eosin (H&E) according to a routine procedure described previously.[65] Images of H&E-stained sections were acquired with a Carl Zeiss Axiocam camera at 200× magnification. The percentage of myofibers with centrally located nuclei and Feret diameter was determined from transverse sections of H&E-stained muscles on five random fields of view per section per mouse.

In vivo physiological testing in DMDdel8–34 mice

Hanging wire test and grip strength test

The wire hanging and grip strength tests were performed on a monthly basis for each mouse according to the protocol described by Aartsma-Rus and van Putten.[66] A 55-cm-wide, 2-mm-thick metallic wire was installed 37 cm above a layer of bedding. Each mouse was given three trials to hang on the wire by the forelimbs with a 30-s recovery period between trials. The maximum hanging time of the three trials was recorded and used as an outcome measure. Grip strength was quantified using the Grip Strength Test Meter for Mice and Rats (IITC Life Science, USA). Grip measurements were replicated 5 times each session, with intervals of a minimum of 1 min between replicates, and mean values were used for the analysis.

Rotarod performance test

The rotarod running test was performed for each mouse every 4 weeks according to a published protocol[66] on a rotarod apparatus for mice and rats (IITC Life Science). First, mice were placed on tubes rotating at 5 rpm, after which the speed was increased to 45 rpm for 15 s. The running time was continuously recorded and stopped when a mouse fell off the tube. Then, the mice were given two more attempts to run. The test session ended for mice that could run for 500 s. The maximum running time was recorded.

Weight test

The weight test was performed for each mouse every 4 weeks according to a described protocol.[67] Briefly, we used weights of 7 different masses (20 g, 28 g, 36 g, 44 g, 52 g, 60 g, and 68 g) fixed on a ball of tangled fine wire. The mouse was allowed to grab the weight with its forelimbs and lift, after which the holding time was recorded. Holding for 3 s is a criterion for passing the test. After resting for 30 s, the test is carried out with a heavier weight. Three attempts were performed when the mouse did not grab the weight. The final total score is calculated as the product of the number of weights held for the entire 3 s multiplied by the holding time (seconds).

Measurement of isometric force and muscle susceptibility to eccentric contraction-induced injury

Measurements of isometric muscle force and susceptibility to eccentric contraction-induced injury were performed for each mouse at the end of the experiment according to the protocols described earlier.[63] First, the tested muscle was adjusted to an optimum length (Lo) to produce the maximum tetanic force. Then, while held at Lo, the muscle was stimulated every 2 min at increasing frequencies (10–250 Hz) to generate force frequency curves to obtain the maximal tetanic force (Po). Then, Lo and muscle mass were recorded and used to normalize to the physiological cross-sectional area (CSA; [Lo × density]/mass) and calculate specific tetanic force (sPo) based on previous protocols (see SOP DMD_M.2.2.005). In the eccentric contraction protocol, the force deficit at each lengthening contraction (P1–P7 = Pn, P1 = Po) was calculated as (Po − Pn)/Po × 100%.

Heart dobutamine test

The mice were sedated with xylazine-tiletamine-zolazepama and placed on the heated surgical table. A catheter with an outer diameter of 0.3 mm was introduced into the left ventricle via the right carotid artery. Next, the intracardiac catheter was connected to a micropressure transducer (Biopac Systems, USA) to dynamically measure systolic and diastolic left ventricular pressure (LVP). When the constant pressure curve had been detected, mice were intravenously administered dobutamine hydrochloride (Sigma-Aldrich, 49745-95-1) at a dose of 5 μg/g body weight or approximately 150 μg per mouse[68] via the tail vein. The output pressure parameters were used to evaluate the dobutamine-induced systolic LVP increase.

Diaphragm contraction test

The diaphragms of exsanguinated mice were thoroughly separated to cut equal 5 mm × 2 mm muscle strips (perpendicular to the ribs) as described previously.[69] Tissue strips were aligned between two holders, and the upper one was connected to a tensometric sensor (Biopac Systems), whereas the lower one created a 0.5-g load. Held diaphragm strips were submerged in Krebs-Henseleit solution (118 mM NaCl, 4.7 mM KCl, 1.18 mM KH_2PO_4, 1.2 mM $MgSO_4$, 2.5 mM $CaCl_2$, 25 mM $NaHCO_3$, and 5.55 mM glucose [pH 7.4]) heated up to 30°C. When the baseline tension curve (g) was obtained, the diaphragm strips were electrostimulated with the following parameters: 100 Hz, 5 V, one time per second for 1 min. The output tension curve was used to calculate the ratio between the initial force and endpoint force or "force deficit," the parameter reflecting exhaustion of the diaphragm contractile reserve.[70]

Hydroxyproline levels

The hydroxyproline content was measured according to a published protocol.[71] In brief, portions of diaphragm tissue were weighed, cut to 10 mg, and subjected to lyophilization for 72 h. Peptides and proteins were hydrolyzed to individual amino acids by adding 600 μL of 10 M sodium hydroxide (NaOH) and incubated for 15 h at 100°C. Samples were cooled to room temperature and then neutralized with 600 μL of 10 N HCl. Then, 150 μL of isopropanol was added to each vial, vortexed for 30 s at 1500 rpm, and centrifuged at 13,000 rpm for 5 min.

Supernatant aliquots of 20 μL were added in triplicate to 96-well plates and incubated at 37°C until dry. A collagen standard curve was prepared from serial dilutions of the *trans*-4-hydroxy-L-proline analytical standard (Sigma, 41875-100MG). Finally, 100 μL of 15% (w/v) DMAB (1 M) in 2-propanol in 10 N hydrochloric acid (Ehrlich's solution) was added to each sample, and plates were immediately vortexed. Plates were incubated at 65°C for 20 min and quickly cooled by immersion in cold water to arrest further chromophore generation. The plates were read at 540 nm.

Genomic DNA isolation and PCR

Genomic DNA was purified from cell culture and frozen tissue samples using the DNeasy Blood & Tissue Kit (QIAGEN) according to the manufacturer's protocol. Cultured cells were scraped out of plastic and resuspended in 200 mkl of PBS. Frozen tissue samples were homogenized using TissueLyser LT (QIAGEN). The concentration was estimated using a NanoPhotometer (Implen), and 100 ng of purified gDNA was used as a template. Guide recognition sites in introns 5 and 34 of the *Dmd* gene, the deletion breakpoint, the internal control gene (*Tet1*), and the top 5 OT sites (Table S2) predicted in the Benchling biology software were amplified with the primers listed in Table S3. We used the Gene Pack PCR Core Kit (Isogene, Russia) or Phire Tissue Direct PCR Master Mix (Thermo Scientific) for amplification. Targeted double-strand break formation was assessed using the mismatch-sensing T7EI enzyme (NEB, M0302 L). Purified from the gel amplicons were denatured for 5 min at 95°C and reannealed by cooling to 85°C (−2°C/s) and then to 25°C (−0.1°C/s). Next, we incubated half of each mixture in 1× NEBuffer 2 and 5 U of T7EI for 1 h at 37°C. The other half was maintained under the same conditions without the enzyme. Then, samples were subjected to electrophoresis through 2.5% (w/v) agarose gels in 1× Tris acetate-EDTA (TAE) buffer. The resulting ethidium bromide-stained DNA species were detected using the iBright FL1500 imaging system (Thermo Fisher Scientific).

qRT-PCR

The total RNA was purified from cells or frozen tissue samples using TRI reagent (MRC) following the manufacturer's recommendation. RNA was additionally treated with DNase I (NEB), and cDNA synthesis was performed using an MMLV-RT kit (Evrogen) and a mix of random and oligo(dT) primers 1:1. PCR for detection of native and shortened cDNA fragments was performed using Mm_dmd-142F and Mm_dmd_ex37R2 primers (Table S3). To assess the shortened transcript percentage, alkaline agarose gel[72] images were analyzed using Fiji software.[73] To quantify the expression rate of a truncated transcript, a forward primer spanning the junction of exons 5 and 35, Mm_dmd_ex5/35F, was used in pair with Mm_dmd_ex37R2. Here and below, the following qPCR conditions were used: 94°C for 3 min, 40 cycles of 94°C for 15 s, 66°C for 15 s, and 72°C for 25 s (+ fluorescence measurement). The copy number of the shortened transcript was defined by calculations from a calibration curve built on pDmdDel6–34 dilutions. Primers and probes specific to reference genes *Rpl13a*, *Ap3d1*, and *Csnk2a2* (Ta = 55°C) were used to normalize gene expression in mice.[74] Dp427 transcripts were amplified by primers designed to the 5′ region preceding mutation and genome editing sites: Mm_dmd_187F to exons 3 and 4 junctions and Mm_dmd_ex5-81R to exon 5 (Ta = 63°C). Dp71 region amplification was performed using primer Dp71-G1-FWD2 to unique exon G1 and Dp71-5′-rev2 to exon 65 (Ta = 64°C). For quantitative analysis, the calibration curve was built on serial dilutions of plasmid DNA containing full-length Dp71 CDS. The full-length Dp71 coding sequence was amplified using the same forward primer and Dp71-fl-Rev to exon 79. The following qPCR conditions were used: 98°C for 3 min; 35 cycles of 98°C for 20 s, 63°C for 30 s, and 72°C for 2 min; and 72°C for 5 min.

5′-RACE

For 5'-RACE analysis, we used one mouse from CRISPR-Cas9-treated and control groups. The total RNA was isolated from frozen muscle samples and reverse transcribed by Mint revertase (Evrogen, SK001) with the specific primer to *Dmd* cDNA, Dp71-fl-Rev. Step-out amplification of upstream *Dmd* sequences was performed with the Mint RACE primer set (Evrogen, SK004) and reverse primers designed for exons 64–66 (Dp71-5′ rev1-3; Table S3). The obtained bulk PCR products were purified from gel and ligated into the pAL-TA vector (Evrogen, TA002) with further transformation of ligation mixes into XL1-Blue cells (Evrogen, CC001). Ten clones for each group were sent for Sanger sequencing.

Sequence analysis

After Sanger sequencing, we analyzed the raw data in Benchling biology software. For quantitative analysis of indel distribution, we utilized TIDE analysis,[27] and DECODR v.3.0 online software[26] was utilized. For TIDE analysis of OT sites, gRNA was entered with corresponding replacements. The indel size ranges were set to 10 nt upstream and downstream of the predicted cut site. A p value of less than 0.01 was accepted as significant. For deletion border analysis and Dp71 splice-variant distribution in DECODR v.3.0, the control sequence was replaced with .fasta file, representing the expected variant. Dual-guide mode and a donor template with spliced exon 71 or 78 were used for splice-variant quantitative analysis.

Western blotting

Cultured cells were collected in reporter lysis buffer (Promega) with cOmplete Protease Inhibitor Cocktail (Roche) and lysed by freezing-thawing. Concentrations were determined using the Bradford method (Quick Start Bradford 1× Dye Reagent, Bio-Rad). Frozen tissue samples were homogenized in RIPA buffer (50 mM Tris [pH 8.0], 150 mM NaCl, 1% Triton X-100, 0.5% sodium deoxycholate, 0.1% SDS, and 0.01% protease inhibitor cocktail) in Tissuelyser LT (QIAGEN). The total protein concentration was measured by a BCA Protein Assay Kit (Sigma) on Clariostar Plus (BMG Labtech). Equal amounts of lysates (up to 50 mkg) were mixed with 4× Laemmli sample buffer, incubated at 95°C for 5 min to denature proteins, and resolved in 8% SDS-PAGE or 4%–15% Mini-PROTEAN TGX Precast Protein Gels (Bio-Rad). Proteins were transferred to a polyvinylidene fluoride (PVDF) membrane (Bio-Rad) using a standard wet transfer protocol in Mini Trans-Blot Cell

(Bio-Rad). Nonspecific binding was blocked by incubating the membrane in 5% dry milk in TBST for 1 h. For dystrophin detection, we used rabbit polyclonal antibodies (Abcam, ab15277, 1:400). To detect the Cas9 protein, we used recombinant anti-CRISPR-Cas9 rabbit antibodies (Abcam, ab203933, 1:20,000). Mouse monoclonal antibodies were utilized for β-dystroglycan identification (Leica Biosystems, USA, NCL-b-DG, 1:200). GFP staining was performed using N-terminal anti-GFP rabbit antibodies (Sigma-Aldrich, G1544-100UG, 1:4,000). GAPDH was used as a loading control (Sigma-Aldrich, ABS16, 1:3,000). Goat anti-rabbit immunoglobulin G (IgG; H+L) cross-adsorbed secondary antibody horseradish peroxidase (HRP; Invitrogen, G-21234, 1:10,000) and goat anti-mouse IgG (H+L)-HRP (Bio-Rad, 1706516, 1:1,500) were used as secondary antibodies. Incubation was carried out overnight at 4°C with primary antibodies and for 1 h at room temperature with secondary antibodies. Signal detection was performed with the Clarity Western ECL Substrate (Bio-Rad) or SuperSignal West Atto Ultimate Sensitivity Substrate (Thermo Scientific). Detection and quantification were performed using the iBright FL1500 scanner (Thermo Fisher Scientific) and iBright analysis software.

Immunofluorescence

Tissues for staining were embedded in Tissue-Tek OCT Compound mounting medium (Sakura Finetek, Japan) and frozen in isopentane (PanReac, Spain) precooled with liquid nitrogen. Ten-micrometer-thick transverse sections were obtained on a CM 1510-1 cryostat (Leica). For laminin/dystrophin and sarcoglycan staining, muscle sections were fixed in 4% paraformaldehyde (PFA; AppliChem, Germany) and 2% D(+)Sucrose (AppliChem) in PBS for 30 min at room temperature and permeabilized in PBST (0.01% Triton X-100 solution in PBS). After permeabilization, nonspecific antibody binding was blocked with 3% bovine serum albumin (BSA; PanEco, Russia) solution in PBST for 1 h at room temperature. Mouse monoclonal antibodies were labeled with biotin (EZ-Link NHS-LC-Biotin, Thermo Scientific, 21336) to avoid internal immunoglobulin staining by secondary antibodies. Instead of PFA, for different dystrophin epitope detection with Mandys105, NCL-Dys2, and Ab15277 antibodies, muscle sections were fixed in acetone:methanol 1:1 for 5 min at room temperature with subsequent blocking in PBS with 3% BSA for 1 h at room temperature. To block endogenous biotin, sections were first covered with 0.1 mg/mL streptavidin (Imtek Russia, S Avs) in PBS for 15 min at room temperature. Then, the excess streptavidin was bound with 0.5 mg/mL D + biotin (BioChemica, A0969) in PBS for 60 min at room temperature. Sections were incubated with rabbit primary antibodies that recognized the dystrophin C terminus (Abcam, ab15277, 1:300), α-sarcoglycan (Abcam, ab189254, 1:2,000), α1-syntrophin (Abcam, ab188873, 1:500), CD68 (Affinity Biosciences, DF7518, 1:100), rat monoclonal antibodies raised against laminin 2α (Abcam, 4H8-2, 1:250), and biotinylated mouse monoclonal antibodies to dystrophin domains (Hybridoma Bank, UK, Mandys105, 1:10; Leica Biosystems, NCL-DYS2, 1:10) at 4°C overnight. Antibodies were diluted in 3% BSA blocking buffer. The following day, the slides were washed and then incubated with Alexa Fluor 488-labeled goat anti-rabbit (Abcam, ab150077, 1:1,000), Alexa Fluor 633-labeled goat anti-rat secondary antibodies (Invitrogen, A21094, 1:1,000), or Alexa Fluor 555-conjugated streptavidin (Invitrogen, S213811, 1:500) for 1 h at room temperature. The cryosections were washed with PBST between each stage. Nuclei were counterstained with Hoechst 33342 (Thermo Fisher Scientific, 1:1,000). Cryosections were mounted in ProLong Gold antifade mounting medium (Invitrogen, P36930). Appropriate negative tissue controls and isotype controls were implemented in the experiments. Fluorescence images were captured on Carl Zeiss LSM 880 and Leica Stellaris 5 confocal microscopes and analyzed in Fiji.[73] Quantitative analysis of α-sarcoglycan staining was performed using CellProfiler 4.2.1 software.[75]

Statistical analysis

Statistical analysis of the results was performed using GraphPad Prism 9 software. Differences identified between groups were determined using ordinary one-way ANOVA or the Kruskal-Wallis test, corrected for Dunnett's or Tukey's multiple comparisons. Differences between the control DMDdel8–34 group and those with $p < 0.05$ are considered significantly different. Data in the text, tables, and graphs are presented as the mean ± standard deviation (SD).

DATA AVAILABILITY

All other data are included in the article or supplemental information and available from the authors upon request. Newly created materials are available from the authors upon request.

SUPPLEMENTAL INFORMATION

Supplemental information can be found online at https://doi.org/10.1016/j.omtm.2023.06.006.

ACKNOWLEDGMENTS

The authors are grateful to Andrei Nogikh for methodological assistance in working with animals and Muhammad David Z. Naimzade for participation in biochemical experiments. Work with animals was carried out on the basis of the Laboratory of Genetic Technologies and Gene Editing for Biomedicine and Veterinary Medicine of the National Research University "BelSU." We thank the Center for Precision Genome Editing and Genetic Technologies for Biomedicine (Institute of Gene Biology), supported by the Ministry of Science and Higher Education of the Russian Federation (075-15-2019-1661), for providing the equipment. The research was done using the equipment of the Core Centrum of the Institute of Developmental Biology RAS. This work was done in Moscow, Russia.

AUTHOR CONTRIBUTIONS

Conceptualization, project administration, and writing – original draft, T.V.E.; methodology, investigation, formal analysis, and visualization, T.V.E., A.V.P., S.G.V., M.A.D., I.M.S., O.A.V., A.A.S., and V.O.S.; supervision, validation, and writing – review & editing, T.V.E., M.V.P., A.V.D., and M.V.B. All authors read and approved the final manuscript.

DECLARATION OF INTERESTS

The authors declare no competing interests.

REFERENCES

1. Doorenweerd, N., Mahfouz, A., van Putten, M., Kaliyaperumal, R., t' Hoen, P.A.C., Hendriksen, J.G.M., Aartsma-Rus, A.M., Verschuuren, J.J.G.M., Niks, E.H., Reinders, M.J.T., et al. (2017). Timing and localization of human dystrophin isoform expression provide insights into the cognitive phenotype of Duchenne muscular dystrophy. Sci. Rep. *7*, 12575. https://doi.org/10.1038/s41598-017-12981-5.

2. Duan, D., Goemans, N., Takeda, S., Mercuri, E., and Aartsma-Rus, A. (2021). Duchenne muscular dystrophy. Nat. Rev. Dis. Prim. *7*, 13. https://doi.org/10.1038/s41572-021-00248-3.

3. Aartsma-Rus, A., Van Deutekom, J.C.T., Fokkema, I.F., Van Ommen, G.-J.B., and Den Dunnen, J.T. (2006). Entries in the Leiden Duchenne muscular dystrophy mutation database: an overview of mutation types and paradoxical cases that confirm the reading-frame rule. Muscle Nerve *34*, 135–144. https://doi.org/10.1002/mus.20586.

4. Bladen, C.L., Salgado, D., Monges, S., Foncuberta, M.E., Kekou, K., Kosma, K., Dawkins, H., Lamont, L., Roy, A.J., Chamova, T., et al. (2015). The TREAT-NMD DMD Global Database: analysis of more than 7,000 Duchenne muscular dystrophy mutations. Hum. Mutat. *36*, 395–402. https://doi.org/10.1002/humu.22758.

5. Takeda, S., Clemens, P.R., and Hoffman, E.P. (2021). Exon-Skipping in Duchenne Muscular Dystrophy. J. Neuromuscul. Dis. *8*, S343–S358. https://doi.org/10.3233/JND-210682.

6. Aslesh, T., Maruyama, R., and Yokota, T. (2018). Skipping Multiple Exons to Treat DMD-Promises and Challenges. Biomedicines *6*, 1. https://doi.org/10.3390/biomedicines6010001.

7. Aoki, Y., Nakamura, A., Yokota, T., Saito, T., Okazawa, H., Nagata, T., and Takeda, S. (2010). In-frame dystrophin following exon 51-skipping improves muscle pathology and function in the exon 52-deficient mdx mouse. Mol. Ther. *18*, 1995–2005. https://doi.org/10.1038/mt.2010.186.

8. Alter, J., Lou, F., Rabinowitz, A., Yin, H., Rosenfeld, J., Wilton, S.D., Partridge, T.A., and Lu, Q.L. (2006). Systemic delivery of morpholino oligonucleotide restores dystrophin expression bodywide and improves dystrophic pathology. Nat. Med. *12*, 175–177. https://doi.org/10.1038/nm1345.

9. Wilton-Clark, H., and Yokota, T. (2023). Recent Trends in Antisense Therapies for Duchenne Muscular Dystrophy. Pharmaceutics *15*, 778. https://doi.org/10.3390/pharmaceutics15030778.

10. Olson, E.N. (2021). Toward the correction of muscular dystrophy by gene editing. Proc. Natl. Acad. Sci. USA *118*. e2004840117. https://doi.org/10.1073/pnas.2004840117.

11. Chen, G., Wei, T., Yang, H., Li, G., and Li, H. (2022). CRISPR-Based Therapeutic Gene Editing for Duchenne Muscular Dystrophy: Advances, Challenges and Perspectives. Cells *11*, 2964. https://doi.org/10.3390/cells11192964.

12. Choi, E., and Koo, T. (2021). CRISPR technologies for the treatment of Duchenne muscular dystrophy. Mol. Ther. *29*, 3179–3191. https://doi.org/10.1016/j.ymthe.2021.04.002.

13. Elangkovan, N., and Dickson, G. (2021). Gene Therapy for Duchenne Muscular Dystrophy. JND *8*, S303–S316. https://doi.org/10.3233/JND-210678.

14. Amoasii, L., Hildyard, J.C.W., Li, H., Sanchez-Ortiz, E., Mireault, A., Caballero, D., Harron, R., Stathopoulou, T.-R., Massey, C., Shelton, J.M., et al. (2018). Gene editing restores dystrophin expression in a canine model of Duchenne muscular dystrophy. Science *362*, 86–91. https://doi.org/10.1126/science.aau1549.

15. Min, Y.-L., Li, H., Rodriguez-Caycedo, C., Mireault, A.A., Huang, J., Shelton, J.M., McAnally, J.R., Amoasii, L., Mammen, P.P.A., Bassel-Duby, R., and Olson, E.N. (2019). CRISPR-Cas9 corrects Duchenne muscular dystrophy exon 44 deletion mutations in mice and human cells. Sci. Adv. *5*, eaav4324. https://doi.org/10.1126/sciadv.aav4324.

16. Maino, E., Wojtal, D., Evagelou, S.L., Farheen, A., Wong, T.W.Y., Lindsay, K., Scott, O., Rizvi, S.Z., Hyatt, E., Rok, M., et al. (2021). Targeted genome editing in vivo corrects a Dmd duplication restoring wild-type dystrophin expression. EMBO Mol. Med. *13*, e13228. https://doi.org/10.15252/emmm.202013228.

17. Duchêne, B.L., Cherif, K., Iyombe-Engembe, J.-P., Guyon, A., Rousseau, J., Ouellet, D.L., Barbeau, X., Lague, P., and Tremblay, J.P. (2018). CRISPR-Induced Deletion with SaCas9 Restores Dystrophin Expression in Dystrophic Models In Vitro and In Vivo. Mol. Ther. *26*, 2604–2616. https://doi.org/10.1016/j.ymthe.2018.08.010.

18. Chemello, F., Chai, A.C., Li, H., Rodriguez-Caycedo, C., Sanchez-Ortiz, E., Atmanli, A., Mireault, A.A., Liu, N., Bassel-Duby, R., and Olson, E.N. (2021). Precise correction of Duchenne muscular dystrophy exon deletion mutations by base and prime editing. Sci. Adv. *7*, eabg4910. https://doi.org/10.1126/sciadv.abg4910.

19. Pickar-Oliver, A., Gough, V., Bohning, J.D., Liu, S., Robinson-Hamm, J.N., Daniels, H., Majoros, W.H., Devlin, G., Asokan, A., and Gersbach, C.A. (2021). Full-length dystrophin restoration via targeted exon integration by AAV-CRISPR in a humanized mouse model of Duchenne muscular dystrophy. Mol. Ther. *29*, 3243–3257. https://doi.org/10.1016/j.ymthe.2021.09.003.

20. Colella, P., Ronzitti, G., and Mingozzi, F. (2018). Emerging Issues in AAV-Mediated In Vivo Gene Therapy. Mol. Ther. Methods Clin. Dev. *8*, 87–104. https://doi.org/10.1016/j.omtm.2017.11.007.

21. van Deutekom, J.C., Bremmer-Bout, M., Janson, A.A., Ginjaar, I.B., Baas, F., den Dunnen, J.T., and van Ommen, G.J. (2001). Antisense-induced exon skipping restores dystrophin expression in DMD patient derived muscle cells. Hum. Mol. Genet. *10*, 1547–1554. https://doi.org/10.1093/hmg/10.15.1547.

22. Erkut, E., and Yokota, T. (2022). CRISPR Therapeutics for Duchenne Muscular Dystrophy. Int. J. Math. Stat. *23*, 1832. https://doi.org/10.3390/ijms23031832.

23. Egorova, T.V., Zotova, E.D., Reshetov, D.A., Polikarpova, A.V., Vassilieva, S.G., Vlodavets, D.V., Gavrilov, A.A., Ulianov, S.V., Buchman, V.L., and Deykin, A.V. (2019). CRISPR/Cas9-generated mouse model of Duchenne muscular dystrophy recapitulating a newly identified large 430 kb deletion in the human *DMD* gene. Dis. Model. Mech. *12*, dmm037655. https://doi.org/10.1242/dmm.037655.

24. Danilov, K.A., Vassilieva, S.G., Polikarpova, A.V., Starikova, A.V., Shmidt, A.A., Galkin, I.I., Tsitrina, A.A., Egorova, T.V., Orlov, S.N., and Kotelevtsev, Y.V. (2020). In vitro assay for the efficacy assessment of AAV vectors expressing microdystrophin. Exp. Cell Res. *392*, 112033. https://doi.org/10.1016/j.yexcr.2020.112033.

25. Wang, D., Zhong, L., Nahid, M.A., and Gao, G. (2014). The potential of adeno-associated viral vectors for gene delivery to muscle tissue. Expet Opin. Drug Deliv. *11*, 345–364. https://doi.org/10.1517/17425247.2014.871258.

26. Bloh, K., Kanchana, R., Bialk, P., Banas, K., Zhang, Z., Yoo, B.-C., and Kmiec, E.B. (2021). Deconvolution of Complex DNA Repair (DECODR): Establishing a Novel Deconvolution Algorithm for Comprehensive Analysis of CRISPR-Edited Sanger Sequencing Data. CRISPR J. *4*, 120–131. https://doi.org/10.1089/crispr.2020.0022.

27. Brinkman, E.K., Chen, T., Amendola, M., and van Steensel, B. (2014). Easy quantitative assessment of genome editing by sequence trace decomposition. Nucleic Acids Res. *42*, e168. https://doi.org/10.1093/nar/gku936.

28. Graham, K.M., Singh, R., Millman, G., Malnassy, G., Gatti, F., Bruemmer, K., Stefanski, C., Curtis, H., Sesti, J., and Carlson, C.G. (2010). Excessive collagen accumulation in dystrophic (mdx) respiratory musculature is independent of enhanced activation of the NF-κB pathway. J. Neurol. Sci. *294*, 43–50. https://doi.org/10.1016/j.jns.2010.04.007.

29. Teramoto, N., Sugihara, H., Yamanouchi, K., Nakamura, K., Kimura, K., Okano, T., Shiga, T., Shirakawa, T., Matsuo, M., Nagata, T., et al. (2020). Pathological evaluation of rats carrying in-frame mutations in the dystrophin gene: A new model of Becker muscular dystrophy. Dis. Model. Mechan. dmm.044701. https://doi.org/10.1242/dmm.044701.

30. Naidoo, M., and Anthony, K. (2020). Dystrophin Dp71 and the Neuropathophysiology of Duchenne Muscular Dystrophy. Mol. Neurobiol. *57*, 1748–1767. https://doi.org/10.1007/s12035-019-01845-w.

31. Lederfein, D., Levy, Z., Augier, N., Mornet, D., Morris, G., Fuchs, O., Yaffe, D., and Nudel, U. (1992). A 71-kilodalton protein is a major product of the Duchenne muscular dystrophy gene in brain and other nonmuscle tissues. Proc. Natl. Acad. Sci. USA *89*, 5346–5350. https://doi.org/10.1073/pnas.89.12.5346.

32. Kawaguchi, T., Niba, E.T.E., Rani, A.Q.M., Onishi, Y., Koizumi, M., Awano, H., Matsumoto, M., Nagai, M., Yoshida, S., Sakakibara, S., et al. (2018). Detection of Dystrophin Dp71 in Human Skeletal Muscle Using an Automated Capillary Western Assay System. Int. J. Math. Stat. *19*, 1546. https://doi.org/10.3390/ijms19061546.

33. Alnassar, N., Borczyk, M., Tsagkogeorga, G., Korostynski, M., Han, N., and Górecki, D.C. (2022). Full-length dystrophin is expressed across human tissues and DMD downregulation commonly occurring in tumours coincides with Duchenne-like molecular alterations. Genetics. https://doi.org/10.1101/2022.04.04.486990.

34. Rani, A.Q.M., Farea, M., Maeta, K., Kawaguchi, T., Awano, H., Nagai, M., Nishio, H., and Matsuo, M. (2019). Identification of the shortest splice variant of Dp71, together with five known variants, in glioblastoma cells. Biochem. Biophys. Res. Commun. *508*, 640–645. https://doi.org/10.1016/j.bbrc.2018.11.168.

35. Farea, M., Rani, A.Q.M., Maeta, K., Nishio, H., and Matsuo, M. (2020). Dystrophin Dp71ab is monoclonally expressed in human satellite cells and enhances proliferation of myoblast cells. Sci. Rep. *10*, 17123. https://doi.org/10.1038/s41598-020-74157-y.

36. Farea, M., Maeta, K., Nishio, H., and Matsuo, M. (2022). Human Dystrophin Dp71ab Enhances the Proliferation of Myoblasts Across Species But Not Human Nonmyoblast Cells. Front. Cell Dev. Biol. *10*, 877612. https://doi.org/10.3389/fcell.2022.877612.

37. González, E., Montañez, C., Ray, P.N., Howard, P.L., García-Sierra, F., Mornet, D., and Cisneros, B. (2000). Alternative splicing regulates the nuclear or cytoplasmic localization of dystrophin Dp71. FEBS Lett. *482*, 209–214. https://doi.org/10.1016/S0014-5793(00)02044-5.

38. Fujimoto, T., Yaoi, T., Fushiki, S., and Itoh, K. (2017). Dp71 is regulated by phosphorylation and ubiquitin-proteasome system in neuronal cells. Biochem. Biophys. Res. Commun. *492*, 349–355. https://doi.org/10.1016/j.bbrc.2017.08.108.

39. Egorova, T., Reshetov, D., Polikarpova, A., Vassilieva, S., Vlodavets, D., and Deikin, A. (2018). DMD treatment: Animal models. Neuromuscul. Disord. *28*, S94. https://doi.org/10.1016/j.nmd.2018.06.251.

40. Nelson, C.E., Wu, Y., Gemberling, M.P., Oliver, M.L., Waller, M.A., Bohning, J.D., Robinson-Hamm, J.N., Bulaklak, K., Castellanos Rivera, R.M., Collier, J.H., et al. (2019). Long-term evaluation of AAV-CRISPR genome editing for Duchenne muscular dystrophy. Nat. Med. *25*, 427–432. https://doi.org/10.1038/s41591-019-0344-3.

41. Zhang, Y., Long, C., Li, H., McAnally, J.R., Baskin, K.K., Shelton, J.M., Bassel-Duby, R., and Olson, E.N. (2017). CRISPR-Cpf1 correction of muscular dystrophy mutations in human cardiomyocytes and mice. Sci. Adv. *3*, e1602814. https://doi.org/10.1126/sciadv.1602814.

42. Bengtsson, N.E., Hall, J.K., Odom, G.L., Phelps, M.P., Andrus, C.R., Hawkins, R.D., Hauschka, S.D., Chamberlain, J.R., and Chamberlain, J.S. (2017). Muscle-specific CRISPR/Cas9 dystrophin gene editing ameliorates pathophysiology in a mouse model for Duchenne muscular dystrophy. Nat. Commun. *8*, 14454. https://doi.org/10.1038/ncomms14454.

43. Singh, S.M., Kongari, N., Cabello-Villegas, J., and Mallela, K.M.G. (2010). Missense mutations in dystrophin that trigger muscular dystrophy decrease protein stability and lead to cross-β aggregates. Proc. Natl. Acad. Sci. USA *107*, 15069–15074. https://doi.org/10.1073/pnas.1008818107.

44. Talsness, D.M., Belanto, J.J., and Ervasti, J.M. (2015). Disease-proportional proteasomal degradation of missense dystrophins. Proc. Natl. Acad. Sci. USA *112*, 12414–12419. https://doi.org/10.1073/pnas.1508755112.

45. Kyrychenko, V., Kyrychenko, S., Tiburcy, M., Shelton, J.M., Long, C., Schneider, J.W., Zimmermann, W.-H., Bassel-Duby, R., and Olson, E.N. (2017). Functional correction of dystrophin actin binding domain mutations by genome editing. JCI Insight *2*, e95918. https://doi.org/10.1172/jci.insight.95918.

46. Banks, G.B., Gregorevic, P., Allen, J.M., Finn, E.E., and Chamberlain, J.S. (2007). Functional capacity of dystrophins carrying deletions in the N-terminal actin-binding domain. Hum. Mol. Genet. *16*, 2105–2113. https://doi.org/10.1093/hmg/ddm158.

47. Echigoya, Y., Nakamura, A., Nagata, T., Urasawa, N., Lim, K.R.Q., Trieu, N., Panesar, D., Kuraoka, M., Moulton, H.M., Saito, T., et al. (2017). Effects of systemic multiexon skipping with peptide-conjugated morpholinos in the heart of a dog model of Duchenne muscular dystrophy. Proc. Natl. Acad. Sci. USA *114*, 4213–4218. https://doi.org/10.1073/pnas.1613203114.

48. Nakamura, A., Fueki, N., Shiba, N., Motoki, H., Miyazaki, D., Nishizawa, H., Echigoya, Y., Yokota, T., Aoki, Y., and Takeda, S. (2016). Deletion of exons 3-9 encompassing a mutational hot spot in the DMD gene presents an asymptomatic phenotype, indicating a target region for multiexon skipping therapy. J. Hum. Genet. *61*, 663–667. https://doi.org/10.1038/jhg.2016.28.

49. Ousterout, D.G., Kabadi, A.M., Thakore, P.I., Majoros, W.H., Reddy, T.E., and Gersbach, C.A. (2015). Multiplex CRISPR/Cas9-based genome editing for correction of dystrophin mutations that cause Duchenne muscular dystrophy. Nat. Commun. *6*, 6244. https://doi.org/10.1038/ncomms7244.

50. Long, C., Li, H., Tiburcy, M., Rodriguez-Caycedo, C., Kyrychenko, V., Zhou, H., Zhang, Y., Min, Y.-L., Shelton, J.M., Mammen, P.P.A., et al. (2018). Correction of diverse muscular dystrophy mutations in human engineered heart muscle by single-site genome editing. Sci. Adv. *4*, eaap9004. https://doi.org/10.1126/sciadv.aap9004.

51. Zhang, Y., Li, H., Min, Y.-L., Sanchez-Ortiz, E., Huang, J., Mireault, A.A., Shelton, J.M., Kim, J., Mammen, P.P.A., Bassel-Duby, R., and Olson, E.N. (2020). Enhanced CRISPR-Cas9 correction of Duchenne muscular dystrophy in mice by a self-complementary AAV delivery system. Sci. Adv. *6*, eaay6812. https://doi.org/10.1126/sciadv.aay6812.

52. Tabebordbar, M., Lagerborg, K.A., Stanton, A., King, E.M., Ye, S., Tellez, L., Krunnfusz, A., Tavakoli, S., Widrick, J.J., Messemer, K.A., et al. (2021). Directed evolution of a family of AAV capsid variants enabling potent muscle-directed gene delivery across species. Cell *184*, 4919–4938.e22. https://doi.org/10.1016/j.cell.2021.08.028.

53. Wieneke, S., Heimann, P., Leibovitz, S., Nudel, U., and Jockusch, H. (2003). Acute pathophysiological effects of muscle-expressed Dp71 transgene on normal and dystrophic mouse muscle. J. Appl. Physiol. *95*, 1861–1866. https://doi.org/10.1152/japplphysiol.00326.2003.

54. Urasawa, N., Wada, M.R., Machida, N., Yuasa, K., Shimatsu, Y., Wakao, Y., Yuasa, S., Sano, T., Nonaka, I., Nakamura, A., and Takeda, S. (2008). Selective Vacuolar Degeneration in Dystrophin-Deficient Canine Purkinje Fibers Despite Preservation of Dystrophin-Associated Proteins With Overexpression of Dp71. Circulation *117*, 2437–2448. https://doi.org/10.1161/CIRCULATIONAHA.107.739326.

55. Lim, K.R.Q., Shah, M.N.A., Woo, S., Wilton-Clark, H., Zhabyeyev, P., Wang, F., Maruyama, R., Oudit, G.Y., and Yokota, T. (2021). Natural History of a Mouse Model Overexpressing the Dp71 Dystrophin Isoform. Int. J. Math. Stat. *22*, 12617. https://doi.org/10.3390/ijms222312617.

56. Leibovitz, S., Meshorer, A., Fridman, Y., Wieneke, S., Jockusch, H., Yaffe, D., and Nudel, U. (2002). Exogenous Dp71 is a dominant negative competitor of dystrophin in skeletal muscle. Neuromuscul. Disord. *12*, 836–844. https://doi.org/10.1016/S0960-8966(02)00141-4.

57. Atencia-Fernandez, S., Shiel, R.E., Mooney, C.T., and Nolan, C.M. (2015). Muscular dystrophy in the Japanese Spitz: an inversion disrupts the *DMD* and *RPGR* genes. Anim. Genet. *46*, 175–184. https://doi.org/10.1111/age.12266.

58. Barthélémy, I., Calmels, N., Weiss, R.B., Tiret, L., Vulin, A., Wein, N., Peccate, C., Drougard, C., Beroud, C., Deburgrave, N., et al. (2020). X-linked muscular dystrophy in a Labrador Retriever strain: phenotypic and molecular characterisation. Skelet. Muscle *10*, 23. https://doi.org/10.1186/s13395-020-00239-0.

59. Moretti, A., Fonteyne, L., Giesert, F., Hoppmann, P., Meier, A.B., Bozoglu, T., Baehr, A., Schneider, C.M., Sinnecker, D., Klett, K., et al. (2020). Somatic gene editing ameliorates skeletal and cardiac muscle failure in pig and human models of Duchenne muscular dystrophy. Nat. Med. *26*, 207–214. https://doi.org/10.1038/s41591-019-0738-2.

60. Percie du Sert, N., Ahluwalia, A., Alam, S., Avey, M.T., Baker, M., Browne, W.J., Clark, A., Cuthill, I.C., Dirnagl, U., Emerson, M., et al. (2020). Reporting animal research: Explanation and elaboration for the ARRIVE guidelines 2.0. PLoS Biol. *18*, e3000411. https://doi.org/10.1371/journal.pbio.3000411.

61. Labun, K., Montague, T.G., Gagnon, J.A., Thyme, S.B., and Valen, E. (2016). CHOPCHOP v2: a web tool for the next generation of CRISPR genome engineering. Nucleic Acids Res. *44*, W272–W276. https://doi.org/10.1093/nar/gkw398.

62. Ran, F.A., Cong, L., Yan, W.X., Scott, D.A., Gootenberg, J.S., Kriz, A.J., Zetsche, B., Shalem, O., Wu, X., Makarova, K.S., et al. (2015). In vivo genome editing using Staphylococcus aureus Cas9. Nature *520*, 186–191. https://doi.org/10.1038/nature14299.

63. Starikova, A.V., Skopenkova, V.V., Polikarpova, A.V., Reshetov, D.A., Vassilieva, S.G., Velyaev, O.A., Shmidt, A.A., Savchenko, I.M., Soldatov, V.O., Egorova, T.V., and Bardina, M.V. (2022). Therapeutic potential of highly functional codon-optimized microutrophin for muscle-specific expression. Sci. Rep. *12*, 848. https://doi.org/10.1038/s41598-022-04892-x.

64. Morcos, P.A., Li, Y., and Jiang, S. (2008). Vivo-Morpholinos: A non-peptide transporter delivers Morpholinos into a wide array of mouse tissues. Biotechniques *45*, 613–614. https://doi.org/10.2144/000113005.

65. Slaoui, M., Bauchet, A.-L., and Fiette, L. (2017). Tissue Sampling and Processing for Histopathology Evaluation. In Drug Safety Evaluation Methods in Molecular Biology, J.-C. Gautier, ed. (Springer New York), pp. 101–114. https://doi.org/10.1007/978-1-4939-7172-5_4.

66. Aartsma-Rus, A., and van Putten, M. (2014). Assessing Functional Performance in the Mdx Mouse Model. JoVE, 51303. https://doi.org/10.3791/51303.

67. Deacon, R.M. (2013). Measuring the Strength of Mice. JoVE, 2610. https://doi.org/10.3791/2610.

68. Bostick, B., Yue, Y., Long, C., and Duan, D. (2008). Prevention of Dystrophin-Deficient Cardiomyopathy in Twenty-One-Month-Old Carrier Mice by Mosaic Dystrophin Expression or Complementary Dystrophin/Utrophin Expression. Circ. Res. *102*, 121–130. https://doi.org/10.1161/CIRCRESAHA.107.162982.

69. Hakim, C.H., Lessa, T.B., Jenkins, G.J., Yang, N.N., Ambrosio, C.E., and Duan, D. (2019). An improved method for studying mouse diaphragm function. Sci. Rep. *9*, 19453. https://doi.org/10.1038/s41598-019-55704-8.

70. Kennedy, T.L., Guiraud, S., Edwards, B., Squire, S., Moir, L., Babbs, A., Odom, G., Golebiowski, D., Schneider, J., Chamberlain, J.S., and Davies, K.E. (2018). Micro-utrophin Improves Cardiac and Skeletal Muscle Function of Severely Affected D2/mdx Mice. Mol. Ther. Methods Clin. Dev. *11*, 92–105. https://doi.org/10.1016/j.omtm.2018.10.005.

71. Cissell, D.D., Link, J.M., Hu, J.C., and Athanasiou, K.A. (2017). A Modified Hydroxyproline Assay Based on Hydrochloric Acid in Ehrlich's Solution Accurately Measures Tissue Collagen Content. Tissue Eng. Part C Methods *23*, 243–250. https://doi.org/10.1089/ten.tec.2017.0018.

72. Kohlbrenner, E., and Weber, T. (2017). Production and Characterization of Vectors Based on the Cardiotropic AAV Serotype 9. Methods Mol. Biol. *1521*, 91–107. https://doi.org/10.1007/978-1-4939-6588-5_6.

73. Schindelin, J., Arganda-Carreras, I., Frise, E., Kaynig, V., Longair, M., Pietzsch, T., Preibisch, S., Rueden, C., Saalfeld, S., Schmid, B., et al. (2012). Fiji: an open-source platform for biological-image analysis. Nat. Methods *9*, 676–682. https://doi.org/10.1038/nmeth.2019.

74. Wang, X., Zhao, H., Ni, J., Pan, J., Hua, H., and Wang, Y. (2019). Identification of suitable reference genes for gene expression studies in rat skeletal muscle following sciatic nerve crush injury. Mol. Med. Rep. *19*, 4377–4387. https://doi.org/10.3892/mmr.2019.10102.

75. Jones, T.R., Kang, I.H., Wheeler, D.B., Lindquist, R.A., Papallo, A., Sabatini, D.M., Golland, P., and Carpenter, A.E. (2008). CellProfiler Analyst: data exploration and analysis software for complex image-based screens. BMC Bioinf. *9*, 482. https://doi.org/10.1186/1471-2105-9-482.